CONTINUOUS LASER DOPPLER ANEMOMETRY MEASUREMENTS IN THE MIXING LAYER OF AN AXISYMMETRIC JET

by

Noel Nee

A thesis submitted to the Faculty
of the Graduate School of State University
of New York at Buffalo in partial fulfillment
of the requirements for the degree of
Master of Science

December 1982

Table of Contents

ACKNOWLEDGEMENT

The author would like to express his deepest appreciation to his advisor, Professor William K. George, Jr., for he not only provided invaluable guidance and inspiration during the course of research work, but also related real life experience to the philosophy of turbulence. The author believes that the latter contribution carries equal weight with the first part toward the goal of higher education.

The author also wishes to express his gratitude to Dr. Preben Buchhave and the staff of his research group at Disa Elektonik A/S Copenhagen, Denmark for their timely advice and discussion on many occasions. In addition, the author would also like to thank Dr. Lars Lading of the Riso Danish National Laboratory and the students of the Turbulence Research Laboratory at The State University of New York at Buffalo for their constructive comments.

A special thanks must be issued to Mr. Robert B. Suhoke, Jr. and Mr. Ron Humphrey for their unfailing support and encouragement. The love, care and encouragement from the author's family deserve a special recognition.

This list of appreciation would not be complete without

the mention of Mrs. Eileen Graber who typed the entire manuscript and the U.S. Air Force Office of Scientific Research who funded the project under Contract Number F49620 80 C 0053.

ABSTRACT

The experimental investigation reported here is part of a continuing effort to understand the large coherent turbulence structure in the mixing layer of an axisymmetric jet.

The investigated flow regime was restricted to the first four jet diameter downstream from the jet exit. Laser Doppler anemometry and continuous frequency tracking techniques were utilized. The seeding material and method were carefully estimated and selected to satisfy the requirement that the particle follow the flow. The random phase fluctuation (Doppler ambiguity) problem was addressed.

The major task was to study the dropout phenomenon associated with a typical frequency tracker in a turbulent flow. A statistical correlation algorithm was formulated to check the importance of dropout to the flow velocity measurement. Computer interfacing instrumentation was set up to collect data to obtain the correlation coefficient.

The results of the mixing layer measurements proved to satisfy the momemtum equation and agreed well with other investigators findings. The dropout statistics did not appear to correlate strongly with the flow velocity.

LIST OF FIGURES

CHAPTER 1

INTRODUCTION

1.1 General Statement of the Problem

The problem to be investigated here is whether a frequency tracker, incorporated with a laser Doppler anemometer, can be used in the measurement of turbulence in the mixing layer of an air jet facility. If these instruments can be adapted to the experimental environment, the next logical question would be: can reliable data be collected from them? (The major effort here was more oriented toward studying the functionality of the instruments rather than looking for the improvement or development of the instruments.)

1.2 Relevance of the Problem

In 1967 and 1970, Professor J. L. Lumley of the Pennsylvania State University proposed an objective approach to investigating the large scale coherent turbulence structure and its relation to jet noise. The method is called the orthogonal decomposition technique.

In brief, Lumley asks whether a candidate eddy $\phi_i(\underset{\sim}{x},t)$

is occurring in an identifiable manner in a given ensemble of random velocity field $u_i(\underset{\sim}{x},t)$.

In order to test the hypothesis, Lumley proposed projecting ϕ_i onto u_i and then determining the extent to which they were parallel. An experiment to apply these techniques to the turbulent jet mixing layer is being carried out at SUNY/Buffalo in the Turbulence Research Laboratory. Because of the sophistication and complexity of the experiment, a careful selection of instrumentation and measuring techniques must be made prior to the measurement. In addition to the use of conventional hot wire anemometry, laser Doppler anemometry (LDA) has been suggested.

The laser instrument uses the Doppler shift of light scattered from moving particles in the flow to derive velocity information. The major advantage of the LDA over hot wire anemometry is that it requires no obstructing device to be placed in the flow, and the relationship between Doppler frequency and flow velocity is linear.

The effectiveness of this technique has been widely recognized. Some of the problems associated with LDA had been analyzed by George et al.(1973). A more recent piece of work by Buchhave et al.(1978) further identified some special problems that require more research input.

Different signal processors generally introduce different limitations in various applications. While a counter type processor is usually preferred in an air flow study, a frequency tracker is used in most liquid flow measurements. However, if the seeding conditions can be improved, the tracker should work just as well in air flow as in liquid.

The task was to use the existing jet facility and create a workable seeding environment to perform a mixing layer measurement. If the frequency tracker could be shown to be a reliable and practical means of measuring turbulence in air flow, it would be an attractive alternative to counter processor since the Tracker is usually more economical and its analog output is similar to that of hot wire.

1.3 Additional Motive for Investigation

As part of determining the validity of any investigation, the experimental techniques and data interpretation generally play a very important role. Recent work at the Turbulence Research Laboratory (SUNY at Buffalo) on jets and plumes have strongly influenced this view, expecially the work of Beuther (1980)and Baker (1980) who discovered significant problems in the jet and plume

literature.

In the following, Beuther's and Baker's findings will be summarized and related to the motivation of the present investigation:

a) Beuther's Finding -- Hot Wire Data Distortion

In most of turbulent shear flow ($\overline{uv} < 0$), momentum carried by slow moving fluid can exchange relative position with fast moving fluid, thus creating flow reversals around the hot wire which in turn produces nonsense voltages. At the present time, available analog processing techniques in this case do not discriminate nonsense voltages from the rest of the signals. Consequently the bad measuring points can easily be mapped erroneously into U + u and v planes to yield incorrect statistics. Measurements in a turbulent buoyant plume indicated the following:

1) The effect of hot wire distortion occurred 5% of the time at the center line where the local turbulence intensity was a minimum.
2) The peak in Reynold's stresses could have been underestimated by 30%.

3) The turbulent energy dissipation could have been overestimated by as much as 100% at the half velocity point.

4) All the single point statistics could be hopelessly confused.

b) Baker's Findings - Experimental Results vs. Physical Laws

A very important aspect of Baker's numerical modelling of a round jet was to examine the agreement of experimental data with the law of conservation of momentum. The 1967 hot wire measurements of Wygnanski and Fiedler in an axisymmetric jet, whose data was used as reference by many later investigators was shown to lose 40% of its momentum by x/D = 100. In view of these findings, the possible application of the LDA to these flows assures considerable importance.

The questions the present investigation tries to answer are three fold: 1) Do the dropout characteristic of frequency tracker significantly distort the data? 2) If they were appreciably biased, what would be the estimate of error and correction method? 3) Does the Doppler broadening preclude the use of a tracker in such a flow?

The final test of the present work would be: Will the

tracker data satisfy the law of conservation of momentum?

1.4 The Scope of This Investigation

The first aim of this work was to examine the requirement for seeding particles. The particles generated in the flow field must be small enough to follow the flow so that a fundamental basis of measurement was insured. Therefore the order of magnitude of the particle diameter had to be estimated, and then the seeding material and method chosen.

The common problem of LDA Doppler ambiguity would be addressed. The profound effect of random phase fluctuation embedded in the measured quantities to be evaluated and shown to not induce too big an error in order to have meaningful velocity results.

The bridge between theory and experiment has to rely on a correlation algorithm, which, if correctly formulated, could indicate the correlation between the dropout and the flow velocity. A computer program was used to collect the dropout statistics and velocity data. Then through batch processing a correlation coefficient was obtained.

The final test of the validity of tracker data would have to be the laws of nature. The momentum equation was derived to allow graphical evaluation of the experimental data, so that numerical addition of area under the momentum curve would reveal what percent of momentum was conserved.

CHAPTER 2

EXPERIMENTAL DESCRIPTION

2.1 Introduction

This chapter describes the flow facility, instrumentation, and the techniques used during the experimental work.

The investigation was conducted in the mixing layer of the 3 inch diameter isothermal, incompressible, axisymmetric air jet shown schematically in Figure 2.1.1. The spatial position of the measurements were fixed by the cylindrical coordinates X,R,θ, referred to as the axial, transverse and lateral directions respectively.

The measurements of mean and fluctuating quantities were taken at four locations, x/D=1, 2, 3, 4. At each location,traverses were made from the center of the jet radially outwards in the transverse direction until the perimeter of the outer mixing layer was reached.

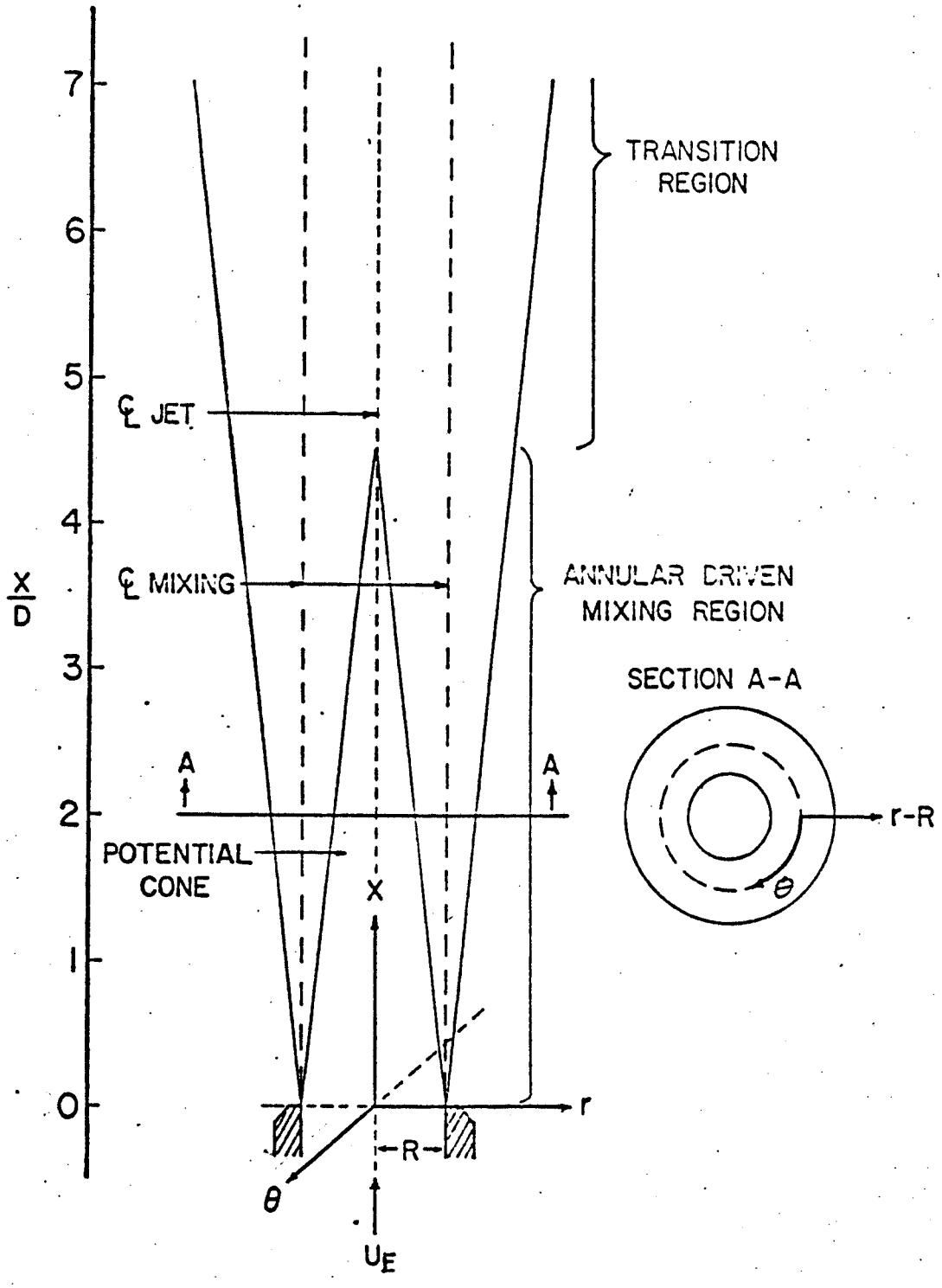

Figure 2.1.1 : Axisymmetric jet coordinate system

2.2 Jet Facility

The jet facility was designed to provide a flat exit profile with a low turbulence intensity and is shown in Figure 2.2.1. The air intake is through a 1/3 hp, single phase fan which could be controlled via a variac. A screened settling chamber and contraction insured that the flow at the exit was free from upstream vibration and flow contamination.

The range of the exit velocity could be varied from 2 m/s to 26 m/s. In order to ensure the flow had a high enough Reynold's number, the velocity was kept at the highest setting. The Reynold's number based on the 3 inch diameter was calculated to be $1.5^{*} \times 10^{5}$.

The air flow was conditioned by passing through a screen diffuser which was designed to transform a rectangular flow into a circular flow section without triggering flow separation. Immediately after this diffuser section was the settling chamber which was divided into four adjoining sub chambers. The swirl was first removed in the honeycomb sub-chamber where hundreds of soda straws (following a suggestion of Nagib) were used instead of the conventional honeycomb plates. The turbulence was further reduced by passing through three sub-chambers divided by

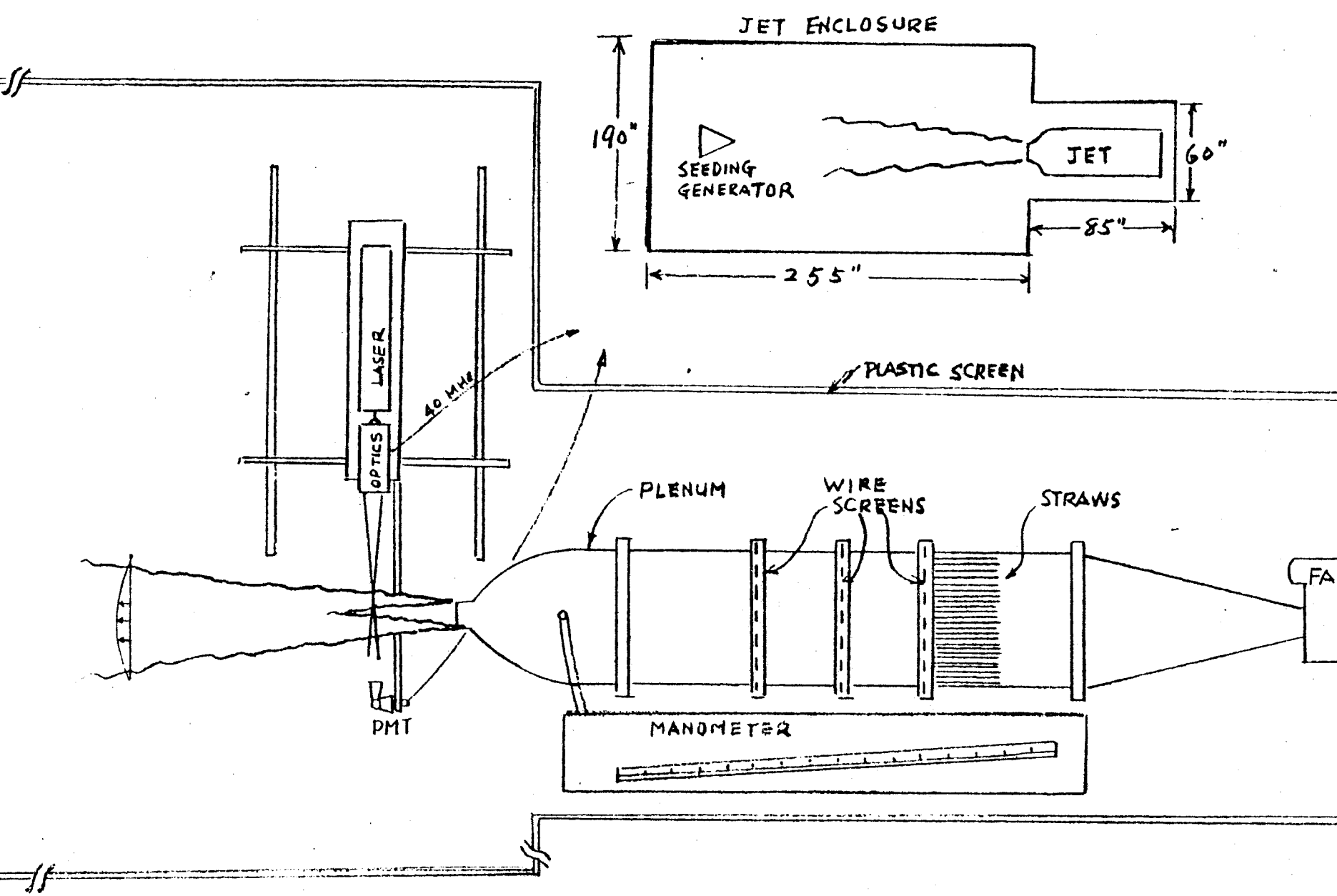

Fig. 2.2.1 Entire jet facility

three wire mesh screens (300 meshes/sq.in.) at the junctions. The flow was finally accelerated through a 16:1 contraction section (having a length to diameter ratio of 1) which had an axial profile of matched cubics designed for minimum pressure gradient (Morel 1975).

The entire jet apparatus was clamped onto a rigid iron table and the eight legs of the table were bolted into the concrete floor.

An inclined type manometer was connected before the contraction section and was used to monitor the velocity head in the jet.

The traversing mechanism consisted of three overlapping aluminum plates which could be traversed by manually sliding them linearly on rails in both axial and transverse directions. The laser and optics were mounted on the top plate. The bottom plate was not movable and thus functioned as the foundation which was bolted on a robust wooden table. Measuring tapes and sliding stops were installed along the rails to permit accurate positioning.

The entire jet experiment was situated in a large and open bay where clean air circulation was maintained and where temperature fluctuations and acoustical contamination

could be kept at a minimum. In order to provide adequate seeding environment, wooden structures were erected and mylar (transparent plastic sheets) were wrapped around the housing frames to enclose the jet facililty as shown in Figure 2.2.1. Considerable space inside the enclosure allowed for both proper entrainment and downstream flow development.

2.3 Initial Nozzle Exit Condition

Although a careful study of the initial conditions at the exit plane of the jet nozzle was not the objective of this investigation, it was important that the flow system be matched to other mixing layer experiments to permit comparisons with earlier and subsequent experiments.

To evaluate the flow system, measurements were carried out at the nozzle exit plane. A constant temperature anemometer (Disa 55M10) and a single sensor hot wire (Disa 55P11) were used to measure the exit conditions. The mean velocity profile shown in Figure 2.2.2 is nearly flat. The background turbulence intensity over the core region was too low to be distinguished from the anemometer noise.

Bradshaw (1966) had shown that mixing layer transition

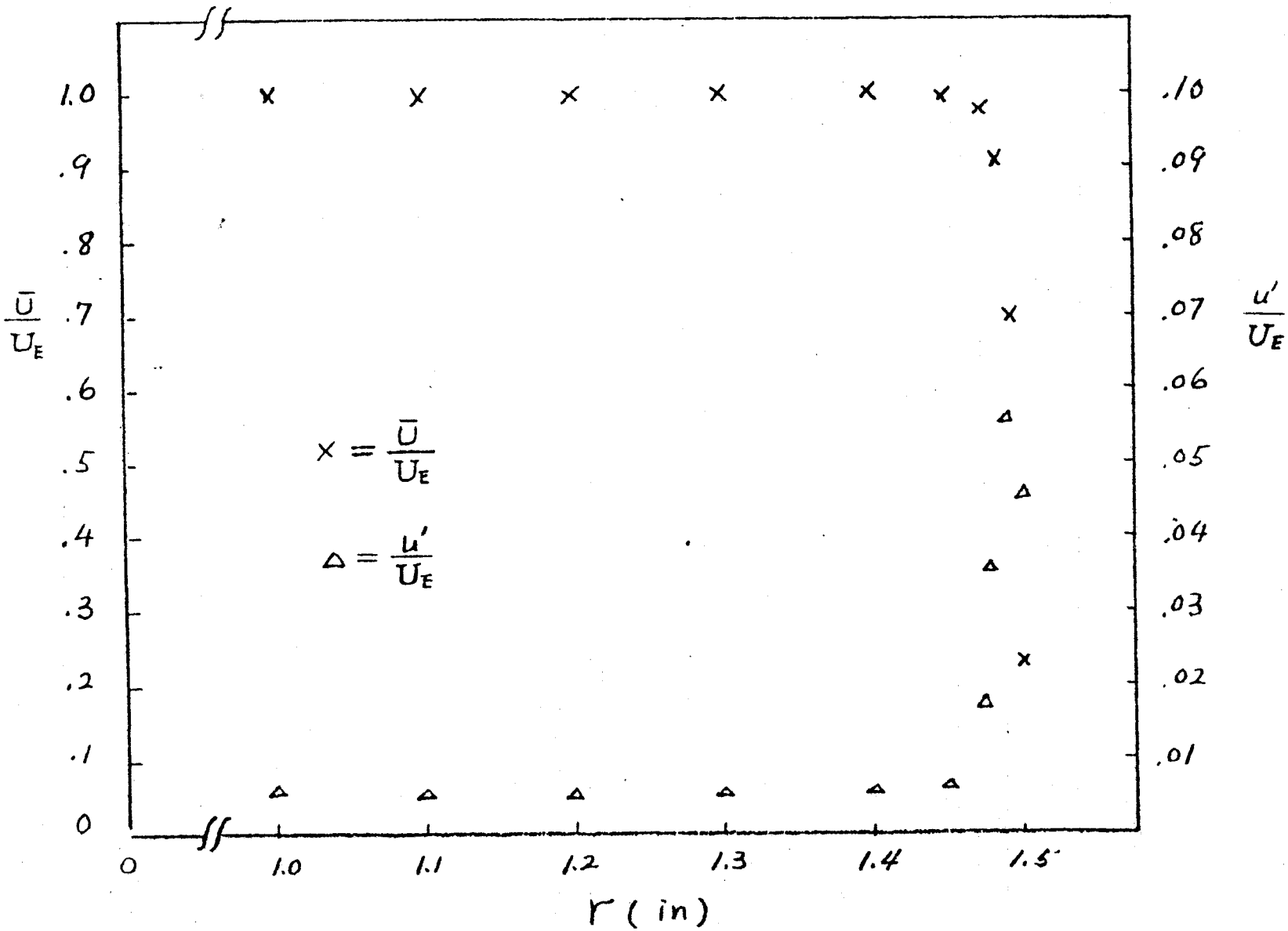

Fig.2.2.2 Mean and RMS velocity profiles at the exit of the jet

and subsequent approach to similarity could be affected by the exit plane boundary layer, the hot wire measurement indicated a laminar boundary layer about 1.3 mm upstream of the exit plane and a approximately self similar mixing layer about one diameter downstream.

In conclusion, a near ideal jet was used in the experiment. The exit profile was nearly flat and of low turbulence intensity. The laminar boundary layer at the lip underwent a rapid transition to a locally self-similar velocity profile in the region where the measurements were concentrated.

2.4 Instrumentation

The velocity measuring system consisted of an optical transducer with optical frequency shift and an electronic processor.

2.4.1 Optical System

Laser light was used as the transmitting medium because of its favorable characteristics (i.e.stability, coherence, monochromaticity and polarization). The transmitting optics

were a Disa 55X modular system, and are schematically shown in Figure 2.4.1. The laser light enters the quarterwave plates, one of which is connected on the laser head to convert the vertically polarized beam into circularly polarized beam, and the other is mounted to the initial optical end and reverts the polarization back to the vertical direction). These allow free rotation of the entire optics without altering the polarization within the unit. The entering beam is then split into two equal intensity beams. One of them passes through the Bragg cell section (a Piezo-electric device that is powered by Disa 55N10 frequency shifter) which creates a 40 MHZ shifted beam relative to the other one which passes through a glass rod in order to maintain equal path length. The next module, the beam translator, displaces the beams with variable beam separation from 13 mm to 39 mm. Lastly, the beams are brought to a focal point in the flow via a front lens. The above mentioned system provides the so-called dual beam fringe mode of operation.

The receiving optics is the part that actually detects the Doppler shifted scattered light from particles that move across the measuring volume. The detector optics not only collects the scattered light, but also defines the solid angle of collection and prevents unwanted light from entering the detection surface. All these functions are

55X MODULAR LDA OPTICS. One-Component Forward Scatter Differential Doppler with Frequency Shifting.

55X51 1 FRONT LENS, Planoconvex (300 mm)
55X08 1 PM SECTION
55X12 1 BEAM EXPANDER
55X21 1 COVER and RETARDER
55X23 2 SUPPORT
55X24 1 BEAM SPLITTER SECTION (Po. Rotator)
55X28 1 BEAM DISPLACER
55X32 1 BEAM TRANSLATOR
55X33 1 LENS MOUNTING RING
55X34 1 PM OPTICS
55X38 1 INTERFERENCE FILTER (633 mm)
55X42 1 MOUNTING BENCH
55X43 1 TRIPOD

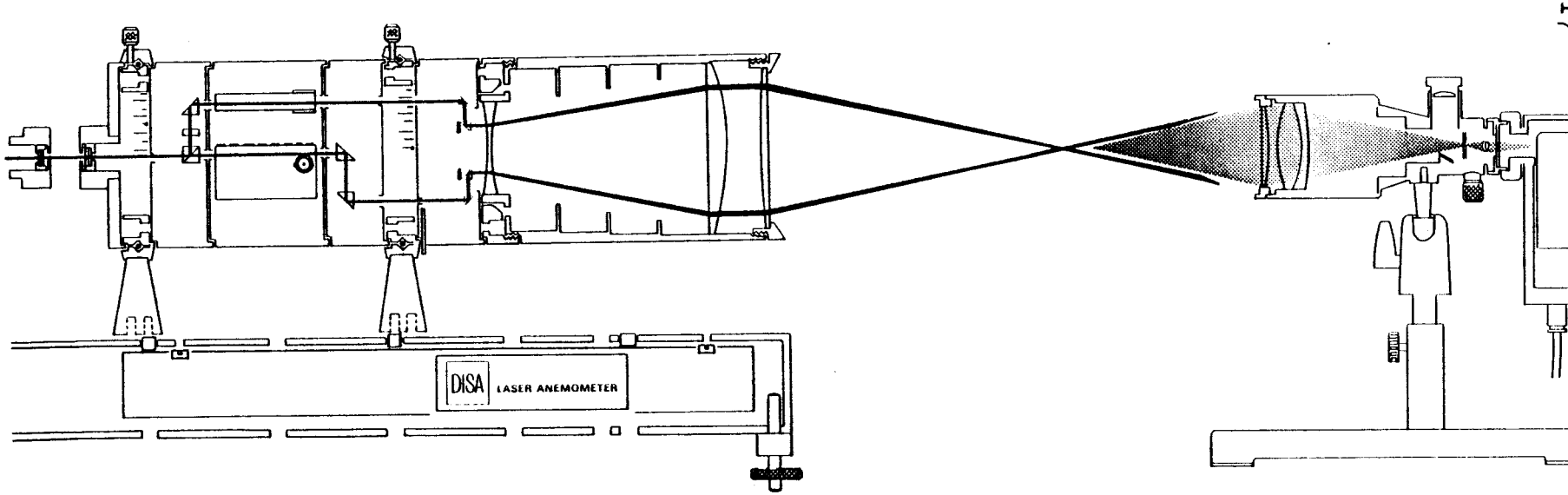

Fig. 2.4.1 Transmitting and Receiving optics layout

then optimized by an imaging technique which creates an actual image of the measuring section of the probe volume onto the pinhole disc, as shown in Figure 2.4.1. The pinhole diameter is small enough, as comparing with the laser wavelength, to fulfill the optical antenna condition (A.E. Siegman, 1966). The field of view of the detector is specified by pinhole diameter and the detector focal length. The adjustment of the pinhole position and a built in eyeport are provided for fine-tuning the detector.

An interference filter is attached to the end of the detector optics to further eliminate unnecessary light that may reach the photodetector where the heterodyning process takes place.

A list of the optical parameters that were described in this section is provided in Table 2.4.

2.4.2 Data Processing System

Two data processing systems were used, one analog and the other digital. The functional block diagram is shown in Figure 2.4.2.

PARAMETERS OF THE OPTICAL SYSTEM:

Laser type : HeNe 15 mW polarized

Front lens : achromat type

Beam diameter, d_1(mm) : 1.1

Wavelength of the laser, λ(mm) : 633

Focal length, f(mm) : 310

Beam expansion ratio, E : 1

Front lens aperture, D(mm) : 79

Detector optics : imaging type with pinhole

Pinhole diameter, r_d(mm) : 0.1

Photodetector : Photomultipier RCA 4526

Bandwidth of the photomultiplier, f_{PM}(MHz) : 120 (3 dB)

Beam separation, D_1(mm) : 39

Half intersection angle, $\theta/2$(deg.) : 3.60

Beam waist diameter, d_f(mm) : 0.23

Probe volume length, 2c(mm) : 3.66

Measuring volume diameter, measured d_{fm}(mm) : 0.3

Measuring volume length, measured d_{lm}(mm) : 4.0

Fringe space, δ_f(um) : 5.04

Fringe number, N_f : 45

Calibration factor, $C = \frac{\lambda}{2 \sin \theta/2} \left(\frac{m\,s^{-1}}{MHz}\right)$: 5.04

Table 2.4 Optical parameters calculated for this experiment

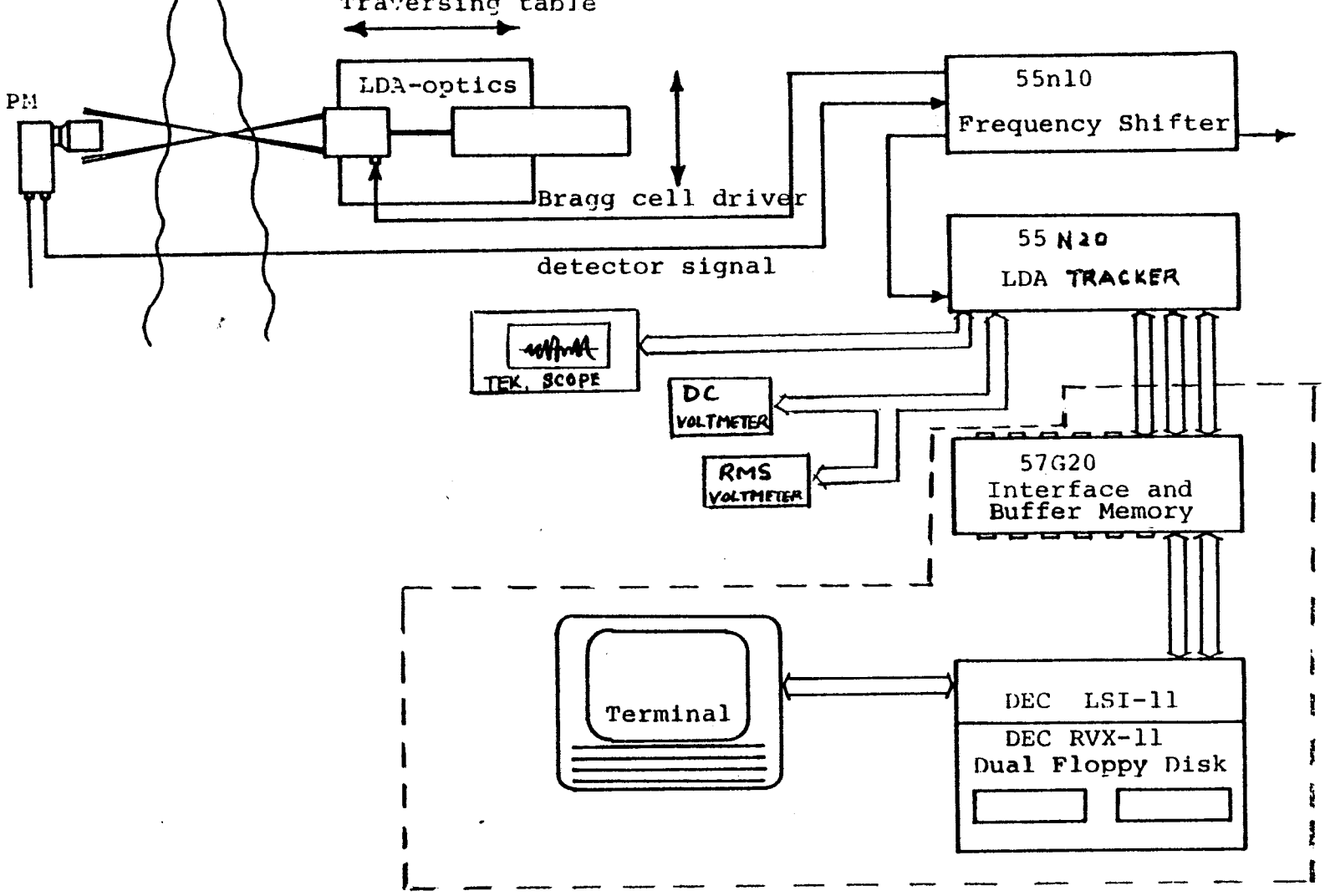

Fig.2.4.2. Block diagram of signal processing equipment.

The major signal analysis device is the Disa 55N20 frequency tracker. It performs a broad band FM demodulation of the Doppler signal. In cases where the signal is dependent on the frequency range, data corresponding to the frequency range of 1KHZ to 10 MHZ ia covered in seven overlapping range.

A phase lock loop is employed in the tracker, as illustrated in Figure 2.4.3a. Its function is to amplify and filter the input Doppler signal. After filtering, the signal is fed to a phase detector (a multiplier circuit), together with the "sine" output from a two phase VCO so that the sine signal lags the input signal 90 degrees. As a result, the VCO will oscillate at the same frequency, say f_T, as the input signal. The biasing input is adjusted in such a way that the VCO will drive towards the middle of the range when out of lock.

The VCO output is the tracker signal which goes to a frequency to voltage converter whereby an analog indication of f_{VCO} is obtained. The F/V converter operates under the charge pump principle and its output is low-pass filtered to remove high frequency variation which may be caused by the noise within the input signal. The low passed output then goes through a sample and hold circuit before it becomes available at the analog out socket.

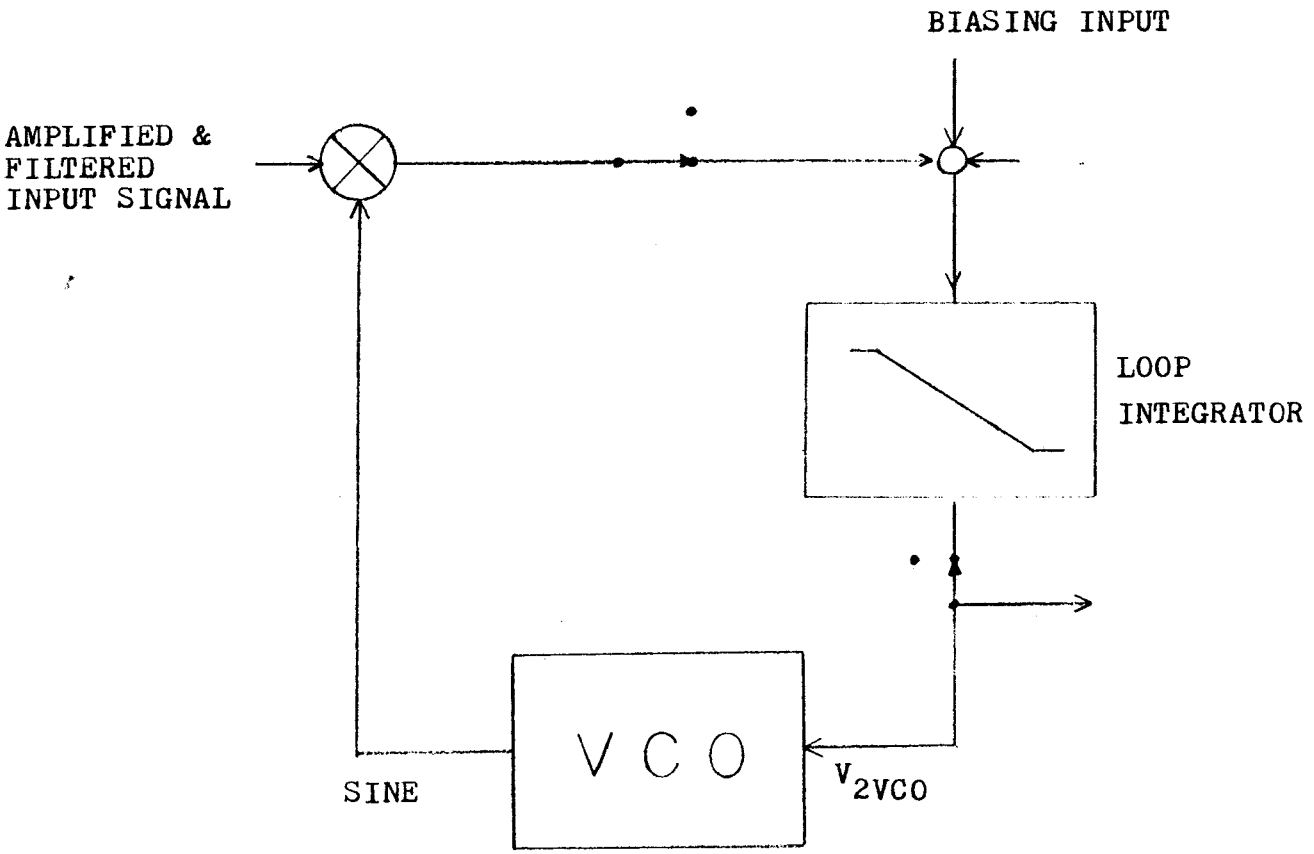

Fig. 2.4.3a Functional block diagram of Phase-Lock-Loop of the Frequency Tracker

The sample and hold circuit is controlled by a lock detector which stops the analog out signal when the tracker is 'out of lock' (the so-called 'drop out') state. The control voltage of the VCO is also available as an output signal but it has much higher bandwidth than that of analog out signal, therefore the noise level is higher.

Another important feature of the tracker is its drop out detection which is determined by the lock detector. If the phase lock loop is "in lock", the amplified input signal will lead the sinusoidal signal from the VCO by 90 degrees. "Lock" can be detected by determining whether the averaged product of the input signal and a cosine signal that is derived from the VCO. If this product is greater than a preset drop-out level then the output signal from the lock detector, L, will go to logic 0 to indicate "lock" and visa versa. When drop-out occurs, an automatic search circuit will break into the phase lock loop in order to get back "in lock" with the signal again.

A great advantage of the frequency tracker is that it is an analog device that can provide analog output for simple analog processing. For example, DC and RMS voltmeters can work with the tracker analog out signal to yield a measurement of mean and fluctuating velocity components in a turbulent flow. This feature bears a close

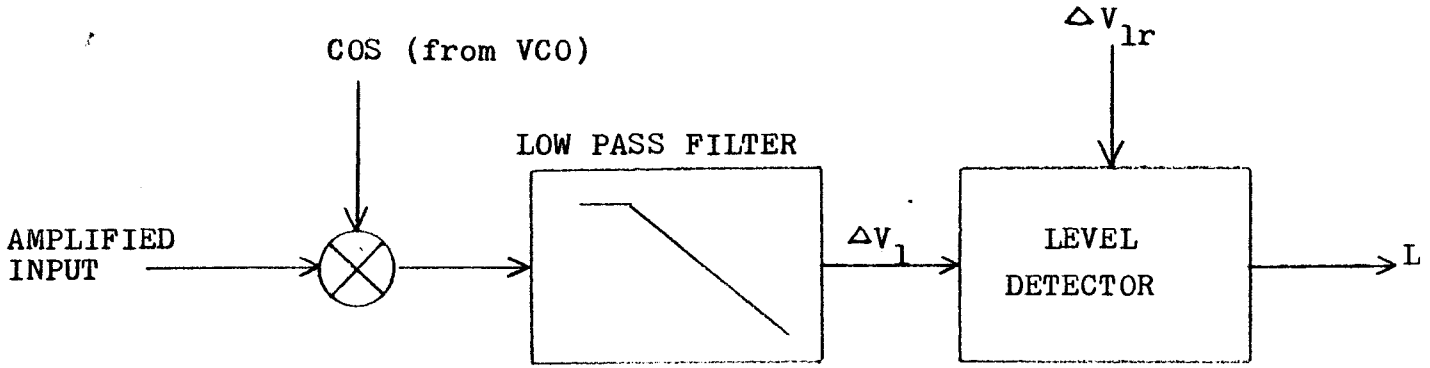

Fig. 2.4.3b Functional block diagram of LOCK DETECTOR of the Frequency Tracker

resemblence to the conventional hot wire anemometer.

An added feature of the Disa tracker is that the analog signal gets routed into period counting circuitry, thereby providing a digital output of the Doppler frequency. More details about this digital sampling method within the tracker will be explained later in the "drop out" analysis section.

2.5 Measuring Procedures and Techniques

2.5.1 Jet LDA Alignment

In the preliminary preparation, aligning the LDA optical system to the jet facility is essential. At first, the axis of the jet had to be determined. For this purpose, two wooden cores were made to fit snugly into the jet nozzle and the diffuser inlet. A hole of about 1.5 mm in diameter was drilled at the center point of each core. The cores were then plugged into the nozzle and the diffuser inlet. A laser was positioned behind the jet to shoot through the center holes of the plugs. In such a fashion, the laser light provided an ideally straight line which was used to represent the center-line of the axisymmetric jet.

The next step was to replace the laser beam by a string which was attached to a point on the center of the nozzle plug (with the plug remaining inside the nozzle) and at a point on the wall about 10m down stream of the jet. Once this hypothetical center line was located, hot wire measurements were taken along the axial and transversal direction using the string as the starting point.

The string was continuously adjusted to follow the maximum mean voltage from the hot wire measurement. As a consequence, although the original position of the string might not have been the true center-line, the final position did correspond to the flow center line.

Finally, the LDA optics were mounted rigidly on the traversing table and then the beams were adjusted to focus on the string. The coalignment of the optics and the jet center was obtained from the exit plane through the x/D=6 point.

2.5.2 Some Operational Consideration

In any type of fluid measurement, the signal-to-noise ratio plays a very important role. The system used in this experiment was selected to provide an optimal S/N ratio,

within the constraints of the experiment.

The forward scatter mode was selected to enhance the intensity of the scattering light. (Usually the intensity of forward scattered light is about 100 times compared with that of back scattered light.)

The pinhole diameter inside the detector optics was only 0.1 mm, thus meeting the coalignment (optical antenna) criterion.

The transmitting optics were chosen to operate in dual fringe mode to eliminate angle dependence.

The receiving optics were supported at the same distance as the focal distance of the front transmitting lens directly opposite of the measuring point, and the optical axis was also tilted about 30 degrees to decrease flare.

A 15 mw laser was used to give adequate power (S/N ratio is proportional to the laser output.)

40mHz optical frequency shift was applied to avoid optical dead angle (see Buchhave 1979).

An approximate shot noise limited state was achieved by taking all the measurements at night (minimum temperature fluctuation in summer time) and in nearly complete darkness (minimum contribution of ambient light).

2.5.3 Seeding Arrangement

One of the criteria to optimize the use of the frequency tracker is that the concentration of seeding particles must be high enough to minimize the signal dropout arising from only sporadic traversals of the light-scattering particles across the measuring volume.

The seeding material was chosen, after a careful analysis, to be glycerine. The particles were generated by simply immersing a soldering iron into a dishful of glycerine to produce smoke. The smoke station was located about 5m downstream at the centerline level. The smoke was recirculated by the jet so that the entire enclosure enclosure was filled before measurements were taken.

The glycerine smoke was generated prior to the measurement so that seeding homogeneity was ensured via visual inspection. Because of the evaporative nature of the glycerine smoke, production of seeding was continued at a

slower rate during the course of measurement.

2.5.4 Velocity Measurement

The velocity measurements began at x/D=1 centerline. Simultaneous analog readings from the analog-out, lock, and mean velocity computer of the tracker were recorded in the transverse direction at 3 mm intervals within the core region of the jet. Near the region of maximum shear in the mixing layer, the measuring interval was decreased to every 1 mm. The transverse scan terminated at the largest radius when the dropout rate reached about 75% and the tracker output could no longer be interpreted.

The same procedure as for the transverse scan was repeated at x/D=2,3,4 and 5. At x/D=5, a potential core was no longer in evidence and the transition to a fully-developed jet was in evidence.

All the analog signals were time-averaged for at least 100 seconds to insure statistical convergence.

CHAPTER 3

SEEDING PARTICLE ANALYSIS

Laser Doppler Anemometers have been used in flow analysis over a wide range of velocities. Controlling the scattering particle concentration and ensuring adequate scattering particle size is always difficult in gases, and presents an especially difficult problem when analog processing techniques are used. It must be remembered that the resulting velocity measurements are actually the measurements of the velocity of randomly distributed particles convected by the motion of the gas. The fundamental requirement for obtaining correct flow velocity data is that the seeding particles must follow the fluid material points without significant lag.

Motion of a single solid or liquid particle in a gas is a simplification of dilute gas solid suspension flow valid at only weak concentrations. We assume this to be the case here. Due to different drag and inertia forces, the larger particles will only follow the large scale flow motions while the smaller particle, if its time constant is small compared to the smallest turbulence time scale, will respond to all the scales of motion. We will begin our analysis by limiting ourselves to spherical particles, and we shall assume that the particles, the fluids, and the flow field

are of such a nature as to make the Reynold's number of the flow around the particles small enough for the Stokes approximation to be valid (i.e. that the particle Reynolds number is much less than unity).

Using the Stokes approximation then, we may write down the Bassett- Boussinesq-Oseen solution for the drag force $F_i[V_i]$ on a particle moving with the velocity $V_i(t)$ in a fluid at rest:

$$F_i[V_i] = -\underset{①}{\frac{2\pi a^3}{3}\rho \dot{V}_i} - \underset{②}{6\pi\mu a}\left\{ V_i + \frac{a}{\sqrt{\pi\nu}} \underset{④}{\int_{-\infty}^{t} d\tau \frac{\dot{V}_i(\tau)}{\sqrt{t-\tau}}} \right\} - \underset{③}{\frac{4\pi a^3}{3}(\rho' - \rho) g_i} \qquad (3.1)$$

where

a	is the radius of the particle
ρ	is the density of the fluid
μ	is the viscosity of the fluid
ν	is the kinematic of the fluid
ρ'	is the density of the particle
g_i	is the gravity factor

Dot indicates differentiation with respect to time. The physical significance of each term is summarized below.

① = apparent mass, same value as given by perfect fluid theory

② = steady state Stokes drag

③ = buoyancy force

④ = unsteady viscous effect, appears to represent a drag due to momentum transferred back to the particle as a "shear wave" from fluid previously accelerated.

Following Tchen (1947) we can superimpose the particle field on a fluid field which has a spatially uniform velocity of $U_i(t)$. The B-B-O solution can be rewritten for the relative particle velocity, $V_i(t)-U_i(t)$. Now following Lumley's analysis (1957), we can express the net force of the entire system (particle and fluid) as

$$F_i[V_i(t)-U_i(t)] + F_i[U_i(t)] = -\frac{4}{3}\pi a^3 \frac{\partial P}{\partial X_i} -$$

$$\frac{2\pi a^3}{3}\rho(\dot{V}_i-\dot{U}_i) - 6\pi\mu a\left\{V_i - U_i + \right.$$

$$\left.\frac{a}{\sqrt{\pi\nu}}\int_{-\infty}^{t} d\tau \frac{\dot{V}_i(\tau)-\dot{U}_i(\tau)}{\sqrt{t-\tau}}\right\} - \frac{4}{3}\pi a^3(\rho'-\rho)g_i \qquad (3.2)$$

The equations of motion of the particle are only valid for a uniform flow field and cannot be directly applied to the non-uniform field in which we are interested. However, if we make the particles small enough compared to the samllest characteristic dimension of the field so that they feel only a quasi steady-state Stokes drag in the direction of the relative velocity, then the general nature of the

uniform field drag expression can be applied in a non-uniform field analysis (see Faxen, Peres and Lumley (1957)).

Let us for simplicity define a function

$$\omega_i(a_j,t) = V_i(a_j,t) - U_i(Y_k(a_j,t),t) \qquad (3.3)$$

where

$Y_k(a_j,t)$ is the particle position at time t

i.e. $Y_k(a_j,0) = a_k$

$$U_i(Y_k(a_j,t),t) = U_i(t)$$

and

$$V_i(a_j,t) = \frac{\partial}{\partial t} Y_j(a_k,t)$$

and neglect the effect of gravity, (i.e. $g_i=0$), since the gravitational force will only produce a constant drift that has no substantial net effect in a strong shear flow.

Then equation (3.2) can be expressed as

$$\dot{\omega}_i + \alpha\omega_i + b\int_{-\infty}^{t} d\tau \frac{\dot{\omega}_i(\tau)}{\sqrt{t-\tau}} = \phi_i(t) \qquad (3.4)$$

where $$K = \frac{9}{2\frac{\rho'}{\rho}+1} \qquad (3.4a)$$

$$\alpha = \frac{\nu K}{a^2} \qquad (3.4b)$$

$$b = \frac{a\alpha}{\sqrt{\pi\nu}} \qquad (3.4c)$$

By following Lumley's suggestion that $\phi_i(t)$ be treated for a moment as a function of time, we shall substitute ω_i with Z_i to eliminate the integral term in equation (3.4).

Now we can write

$$\dot{Z}_i + \alpha \dot{Z}_i = \phi_i(t) \tag{3.5}$$

If we define the Fourier transform of Z(t) and ϕ(t) to be

$$\hat{Z}(\omega) = F.T.\{Z(t)\}$$

$$\hat{\phi}(\omega) = F.T.\{\phi(t)\}$$

we can further transform equation (3.5) to get

$$i\omega\hat{Z} + \alpha\hat{Z} = i\omega\hat{\phi} \tag{3.6}$$

Since α has a dimension of inverse time, we can define a time constant.

$$a_1 = \frac{1}{\alpha} \tag{3.7}$$

By substituting into equation (3.6) and rearrange the terms, it can be shown that

$$\hat{Z} = \left(\frac{i a_1 \omega}{1 + i a_1 \omega}\right)\hat{\phi} \tag{3.8}$$

From linear system theory, we define $H(\omega)$ to be the complex transfer function or the particle frequency response

function:

$$H(\omega) = \frac{i a_1 \omega}{1 + i a_1 \omega} \qquad (3.9)$$

so that the linear expression of particle and fluid point becomes

$$\hat{Z}(\omega) = H(\omega)\,\hat{\phi}(\omega) \qquad (3.10)$$

Obviously equation (3.8) demonstrates a great simplification over equation (3.3) since it involves only $H(\omega)$ which tells us everything we need to know about the system; in particular, how it affects the relation between what we would like to measure, the flow velocity, and what the LDA actually measures, the particle velocity. Thus if the particle frequency response function, $H(\omega)$, is known, all we need is to multiply the Fourier transform of the LDA signal by the inverse of $H(\omega)$ to predict the flow velocity.

By requiring the particle to follow the fluid motion, we mean that the value of the spectrum of particle/fluid relative velocity should be small compared with the value of the spectrum of fluid velocity at the wavenumber in question. Therefore we shall proceed to obtain the $H(\omega)$ through a spectral derivation of equation (3.8).

The spectra of $Z(t)$ and $\phi(t)$ can be acquired by using

the Wiener-Khintchine relation.

The Wiener-Khintchine theorem states that if u(t) is a real and random function of time, then

$$\overline{u(t)\,u(t+\tau)} = \iint_{-\infty}^{\infty} e^{i(\omega t - \omega' t')}\, \overline{\hat{u}^*(\omega')\,\hat{u}(\omega)}\, d\omega\, d\omega'$$

$$= \iint_{-\infty}^{\infty} e^{i(\omega t - \omega' t')} S_{uu}(\omega)\, \delta(\omega - \omega')\, d\omega\, d\omega' \quad (3$$

where τ denotes time lag, * represents the complex conjugate, $s_{uu}(\omega)$ is the spectrum of u(t), and $\delta(\omega-\omega')$ is a Dirac delta function. Thus we can equate

$$S_{uu}(\omega)\,\delta(\omega-\omega')\,d\omega\,d\omega' = \overline{\hat{u}^*(\omega')\,\hat{u}(\omega)}\, d\omega\, d\omega' \quad (3.1$$

or equivalently

$$S_{uu}(\omega)\, d\omega = \begin{cases} \overline{\hat{u}(\omega)\,\hat{u}^*(\omega')}\, d\omega\, d\omega' , & \omega = \omega' \\ 0 , & \omega \neq \omega' \end{cases} \quad (3.13)$$

By carrying out the indicated operation on equation (3.7) it is straight- forward to show that

$$S_{zz}(\omega) = H(\omega)\, H^*(\omega)\, S_{\phi\phi}(\omega)$$

$$= |H(\omega)|^2\, S_{\phi\phi}(\omega)$$

$$= \left(\frac{a_1^2\omega^2}{1+a_1^2\omega^2}\right) S_{\phi\phi}(\omega) \quad (3.14)$$

We can conclude that the effect of the particle lag is to high pass filter the relative velocity at a cut-off frequency corresponding to the particle time constant a_1. Therefore to measure the flow velocity spectrum to a frequency (in a Lagrangian sense) we must ensure that the particle lag satisfies the following condition:

$$(a_1\omega)^2 << 1 \qquad (3.15)$$

Thus equation (3.13) supplies us with a means of estimating the upper limit of the particle size to obtain a given frequency. Alternately given the particle size, equation (3.13) provides a means of estimating the effect on the measurements of the low-pass filtering introduced by the particles in present investigation.

Following Lumley (1976) and taking the fluid velocity seen by the particle to be essentially the Lagrangian velocity, we can measure up to the Kolmogrov microscale if we are able to resolve $\omega_k = .74\frac{v}{\eta}$ (see Fig. 3.1) where $v = (\nu\varepsilon)^{1/4}$ is the Kolmogrov velocity, and $\eta = (\frac{\nu^3}{\varepsilon})^{1/4}$ is the Kolmogrov micro- scale. If we take the specific criterion that the velocity lag error be no more than 1%, then we can write

$$a_1\omega \leq 10^{-2} \qquad (3.16)$$

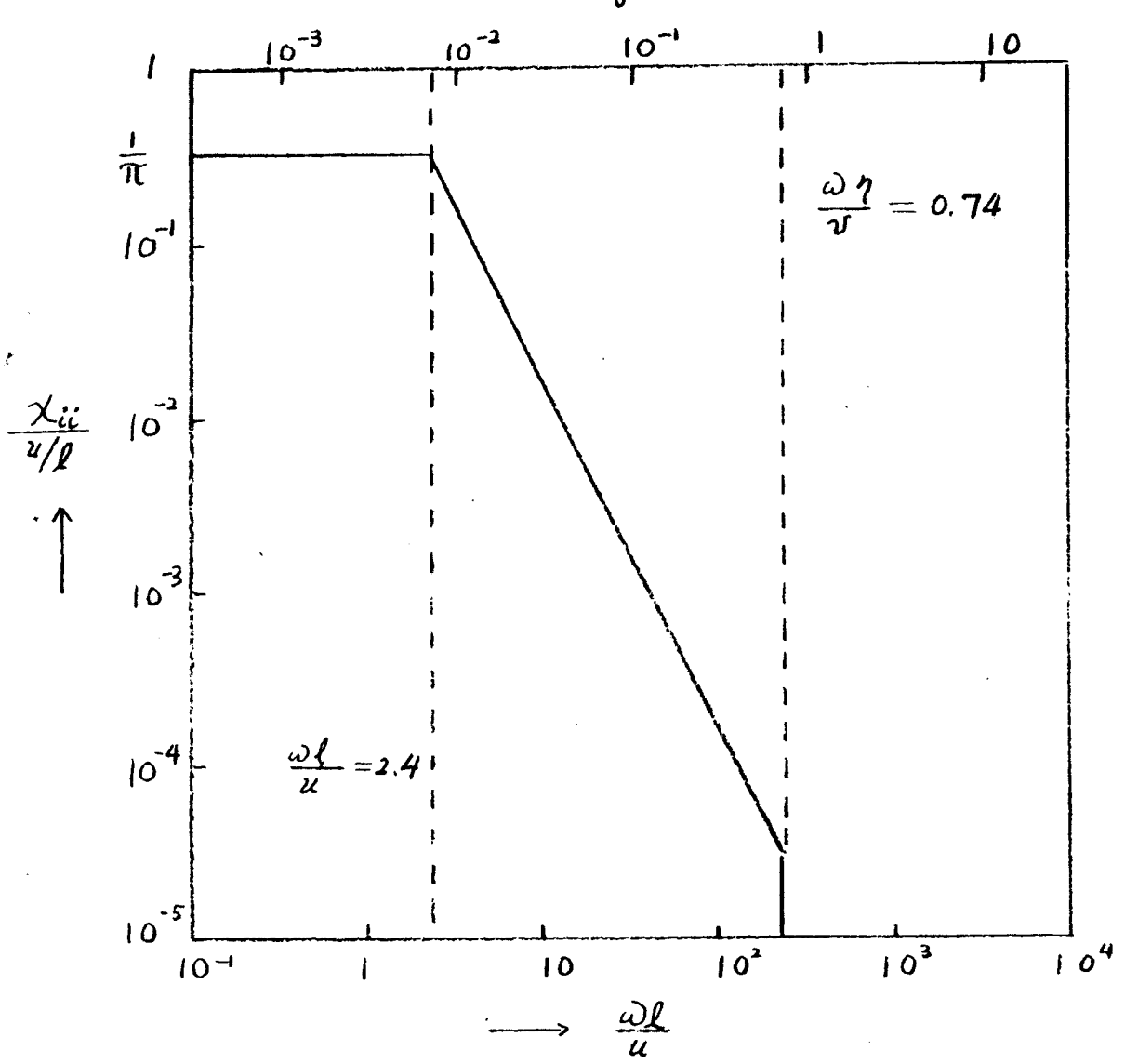

Fig. 3.1 Approximate Lagrangian velocity spectrum for $R_1 \cong 10^5$

now substituting

$$\omega_K = .74 \frac{\nu}{\eta}$$

we get

$$a_1 \left(\frac{\varepsilon}{\nu}\right)^{1/2} \leq \frac{1}{74} \qquad (3.17)$$

One additional piece of information is needed to relate the particle time constant a_1 and particle diameter d. Since a_1 is the inverse of α from equation (3.3), $\alpha = \frac{\nu k}{a^2}$ and

$$k = \frac{9}{2\frac{\rho'}{\rho} + 1}$$

thus

$$a_1 = \frac{1}{\alpha} = \frac{a^2}{\nu\left(\frac{9}{2\frac{\rho'}{\rho}+1}\right)} \qquad (3.18)$$

substituting (3.17) in (3.16), we get

$$\frac{a^2}{9\nu}\left(2\frac{\rho'}{\rho}+1\right)\left(\frac{\varepsilon}{\nu}\right)^{1/4} \leq \frac{1}{74} \qquad (3.19)$$

thus the upper limit on particle diameter to resolve to the Kolmogrov micro-scale is

$$d = 2a = \left[\frac{36}{74}\nu\left(\frac{\nu}{\varepsilon}\right)^{1/4}\left(2\frac{\rho'}{\rho}+1\right)^{-1}\right]^{1/2} \qquad (3.20)$$

From George, Beuther and Arndt (1982), the rate of dissipation of turbulent energy in the mixing layer is

estimated as

$$\varepsilon \sim \frac{u^3}{\ell} \simeq 0.04 \frac{U_E^3}{x}$$

where

U_E = Jet exit velocity = 23 m/s

$x = D_{jet} = 0.076$ m

this gives

$$\varepsilon \simeq 6400 \ m^2/s$$

For all the practical situations, the typical particle-to-fluid density ratio is about 1000, and $\nu_{air} \simeq 10^{-6} m^2/s$, thus the upper limit of the particle diameter is calculated to be 1 micron. Since the glycerine smoke particles are similar to the tobacco smoke which falls in the range of 0.1 to 1.0 micron according to the data collected by Melling and Whitelaw (Fig. 3.2), we should not have problem here.

As an alternate criterion, we might require only that a_1 be sufficiently small so that the measured rms velocity will not be in great error. This is a accomplished by allowing a_1 to occur in the inertial subrange, say

$$\omega = 20 \frac{u}{\ell} \qquad (3.21)$$

Method of generation	Material	Quoted diameter (μm)	Comments
atomisation	water	1–2	evaporation inhibitor added
	DOP	0.35–1.2	commercial atomiser used
	Teflon dust	75% less than 2	atomised from Teflon-Freon suspension
	silicone oil	mostly less than 5	very satisfactory
fluidisation	titanium dioxide	0.5–2	stable in flames up to 2500 C
	geon (PVC)	0.3–0.8	large agglomerates formed; erratic flow
	aluminium, aluminium oxide	up to 8	in solid fuel rocket exhaust, and from fluidised bed in cold flow
chemical reaction	ammonium chloride	1.2	produced from ammonia and hydrogen chloride gases, (which are toxic and corrosive)
	stannic chloride		used in flames, but particles consumed
combustion	tobacco smoke	0.1–1.0	dirty, unsteady flow
	magnesium oxide		from burning of magnesium powder; used in flames
	smoke bombs	over 3	corrosive, toxic, uncontrollable production rate
	smoke pellets	0.03–1.0	commercial product, low flow rate
sublimation	ice	0.5	formed during expansion of humid air through supersonic nozzle

Fig. 3.2 Various aerosol particle sizes applied in LDA

l is defined as

$$l \simeq \frac{u^3}{\varepsilon} \tag{3.22}$$

Thus

$$a_1 < \frac{1}{20}\left(\frac{l}{u}\right) \simeq \frac{1}{20}\left(\frac{\frac{u^3}{\varepsilon}}{u}\right) \tag{3.23}$$

Since $u \simeq 0.16\, U_E$,

$$a_1 < \frac{\frac{1}{20}(0.16)^2 U_E^2 D}{(0.04)\, U_E^3} \tag{3.24}$$

From the values used above, $a_1 \simeq 9.74 \times 10^{-5}$ m

Using equation (3.18) again, we get

$$d = 5\ \mu m$$

Thus we definitely do not have a problem here.

CHAPTER 4

DOPPLER AMBIGUITY ANALYSIS

The measurement of unsteady fluid velocity with LDA always presents a difficulty because of the Doppler ambiguity. The concept of Doppler ambiguity can be illustrated by Fig. 4.1. Basically, the Doppler ambiguity arises from the fact that particles have a finite transit time through the measuring volume which creates a broadened bandwidth in the Doppler spectrum. The phenomenon is called the transit time broadening and it is the predominent ambiguity effect in laminar flow. However, the nature of the turbulent flow introduces additional ambiguity terms to the transit time broadening; in particular, the turbulence broadening and velocity gradient broadening are important.

The turbulence broadening originates from the fluctuating displacement of the particles across the measuring volume. The mean velocity gradient existing in the volume generates the velocity gradient broadening. George and Lumley have discussed the effect of these sources of broadening on the Doppler signal and they demonstrated an exact theory for the Doppler ambiguity for both the Doppler beat signal and its demodulation. The analysis presented here will be based on their results. The aim is not to bring in any technique to correct the spectrum, but mainly

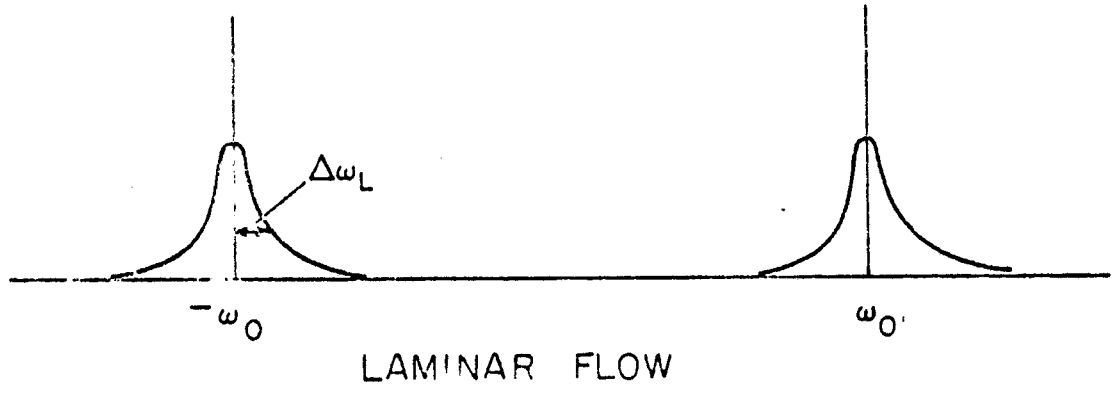

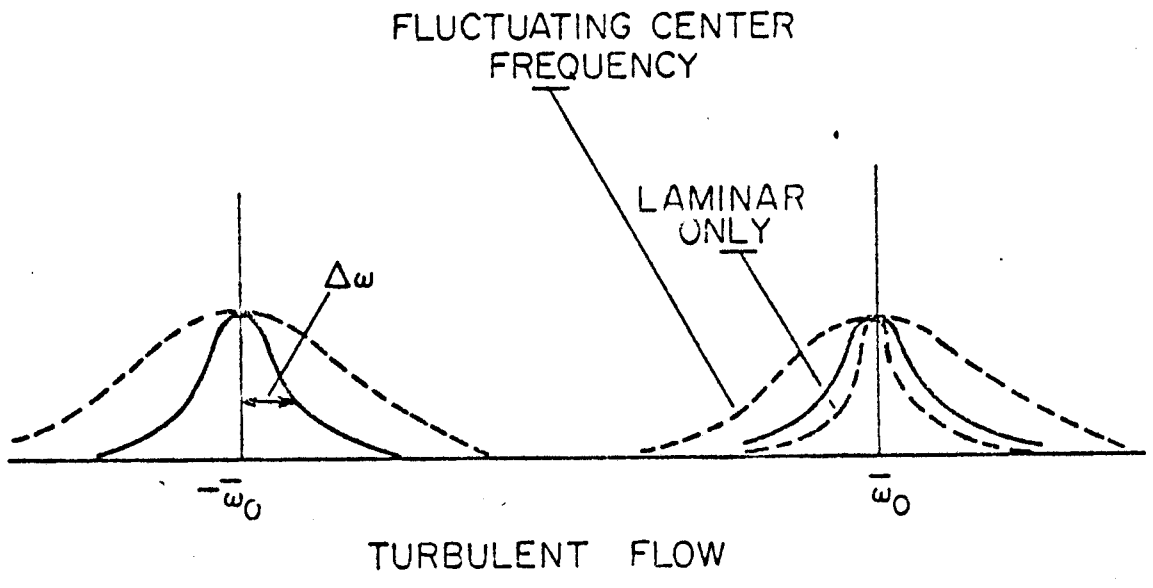

Fig. 4.1 Spectrum of the Doppler Signal Current.

to estimate the contribution of the Doppler ambiguity relative to the turbulence intensity measurement.

Since part of the interest in the present jet experiment is to study the usefulness of the frequency tracker, we will concentrate our effort in analyzing the instantaneous output of the tracker signal; thus we will first look at the demodulated signal.

The mean square demodulated signal may be expressed as:

$$\overline{\omega'^2_{meas}} = K^2 \overline{u'^2} + \overline{\dot{\phi}^2} \qquad (4.1)$$

where $\overline{\omega'^2_{meas}}$ is the measured mean square fluctuating frequency.

$\overline{u'^2}$ is the true mean fluctuating velocity.

$\overline{\dot{\phi}^2}$ is the mean square phase fluctuation due to ambiguity.

K is the scattering wavenumber which is simply Doppler frequency divided by velocity.

The mean square ambiguity fluctuation is in principle infinite (see Fig. 4.2). However, a finite value can be acquired with the use of a low pass filter nevertheless the ambiguity contribution to the overall measured intensity may be significant (if not dominant) since the spectrum of the turbulence and the ambiguity share the same frequency band.

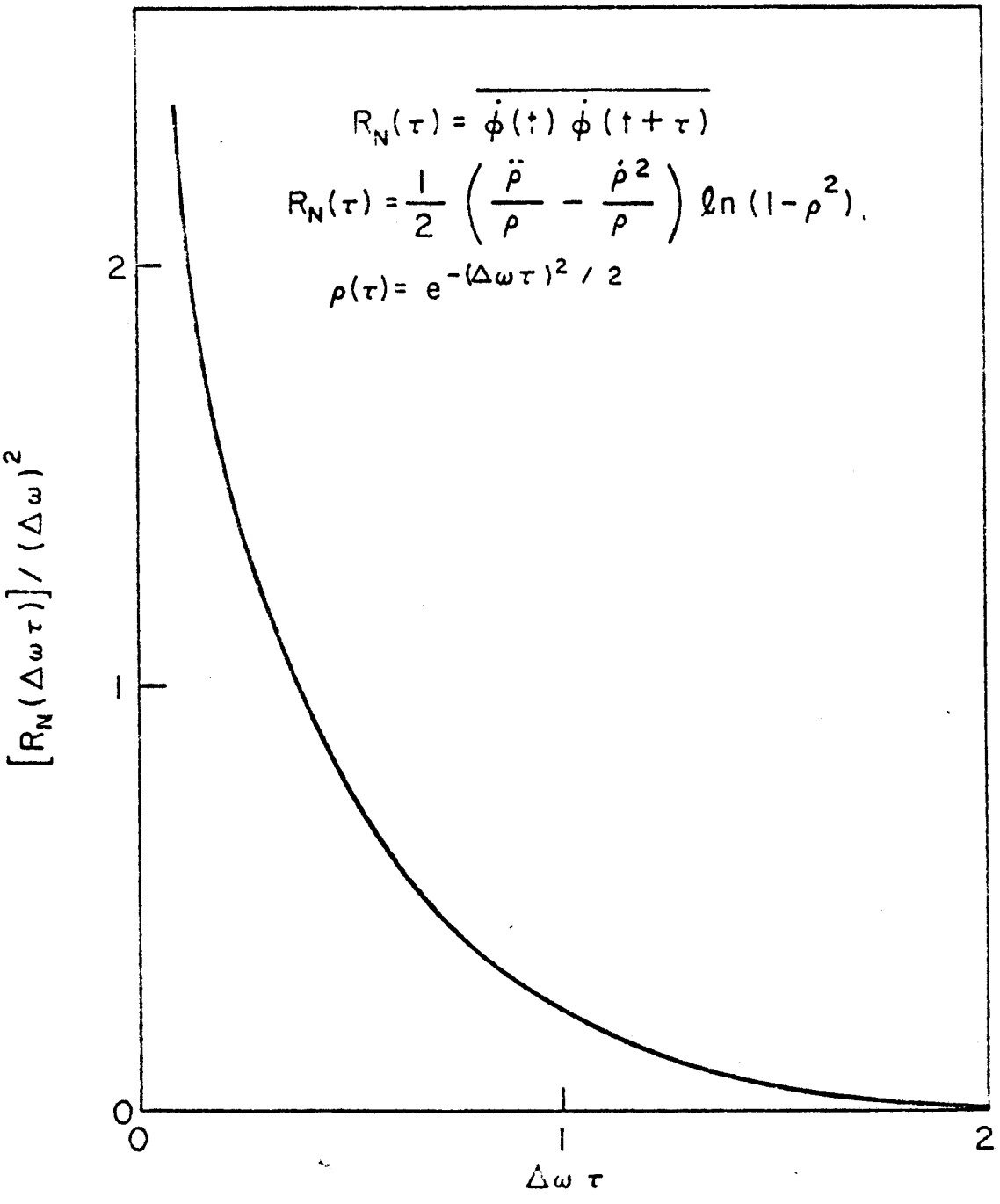

Fig.4.2 Autocorrelation of the Phase Fluctuations, $\overline{\dot{\phi}(t)\dot{\phi}(t+\tau)}$.

This is illustrated Fig. 4.3 as we can see that the contribution of the Doppler ambiguity in the entire intensity measurement can be made as small as we like by using different low pass filters. Unfortunately, the price we have to pay is that the true turbulent fluctuations will also be filtered out. As a result the optimal cutoff frequency of the low pass filter might be chosen at the point where turbulence spectrum equals the ambiguity spectrum.

Following George and Lumley's assumption that the effective scattering volume is small enough, therefore the loss of intensity due to spatial average is not a problem. Then, according to George and Lumley (1973), the spectrum of the demodulated Doppler ambiguity can be given for a Gaussian probe volume as:

$$N(\omega) = \frac{\Delta\omega}{4\sqrt{\pi}} \sum_{n=1}^{\infty} n^{-3/2} e^{\left[\frac{-\omega^2}{4n(\Delta\omega)^2}\right]} \qquad (4.2)$$

where $\Delta\omega$ is the total Doppler ambiguity bandwidth. As shown in Fig. 4.3, if the integral of $N(\omega)$ is taken over all frequencies, the mean square value is infinity, rendering intensity measurement impossible.

Since the low pass filter is used, the spectrum of the demodulated ambiguity has to be modified to show the effect

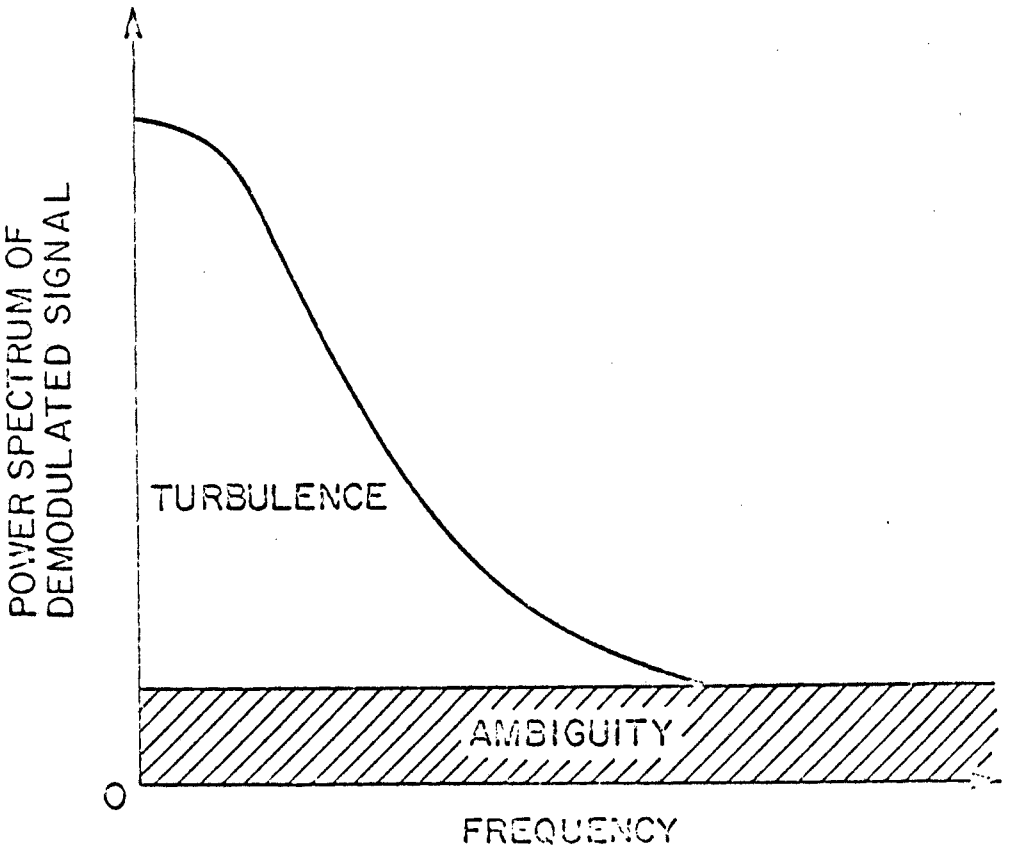

Fig. 4.3 Velocity and Ambiguity Spectrum

of a low passed white noise, a simple R-C circuit gives a respondence function:

$$|H(\omega)|^2 = \frac{1}{1+(\frac{\omega}{\omega_L})^2} \tag{4.3}$$

where $\omega_L = \frac{1}{RC}$ is the cut off frequency.

Then, the low-passed spectrum of the demodulated ambiguity is

$$N_{LP}(\omega) = |H(\omega)|^2 N(\omega)$$

$$= \frac{1}{1+(\frac{\omega}{\omega_L})^2} N(\omega) \tag{4.4}$$

Now it is straightforward to get the mean square low passed phase fluctuation by integrating $N_{LP}(\omega)$ over all frequencies as

$$\overline{\dot{\phi}_{LP}^2} = \int_{-\infty}^{\infty} N_{LP}(\omega)\, d\omega \tag{4.5}$$

To a first order approximation, we can assume $N(\omega) \simeq N(0)$, where N(o) represents the value of the ambiguity spectrum at the origin. George and Lumley give N(o) as $0.368\Delta\omega$. Thus

$$\overline{\dot{\phi}_{LP}^2} = N(0) \int_{-\infty}^{\infty} \frac{1}{1+(\frac{\omega}{\omega_L})^2}\, d\omega$$

$$= 2N(0)\omega_L \int_{-\infty}^{\infty} \frac{1}{1+(\frac{\omega}{\omega_L})^2} \frac{d\omega}{\omega_L}$$

$$= 2N(0)\omega_L [\text{Arc Tan } \omega|_0^{\infty}]$$

$$= 1N(0)\omega_L (\tfrac{\pi}{2})$$

It is convenient to use the circular frequency so we can reexpress equation (4.6) as

$$\overline{\phi'^2_{LP}} = 0.368\,\pi\,(2\pi\Delta f)(2\pi f_{LP}) \qquad (4.7)$$
$$= 45.64\, f_{LP}^2 \text{ , For the worst case.}$$

If the condition

$$\frac{\overline{\phi'^2_{LP}}}{\overline{\omega'^2}_{measured}} << 1 \qquad (4.8)$$

is satisfied, the intensity measurement may be considered accurate.

The next question is at what cut off frequency should one use to optimize the result? This criterion was also set by George and Lumley. Since the ambiguity spectrum will appear in the form of a white noise added to the spectrum, if we know the wavenumber at which the ambiguity and the turbulence spectra are equal, we can place the low passed filter there.

Using Fig. 13 of George and Lumley (see Fig 4.4) and computing in the center of the mixing layer at one diameter downstream:

$\theta = 7.2$, Angle of Intersection

$\bar{u} = 0.6\,\bar{u}_E = 13.8$ m/s

$\lambda = 633 \times 10^{-9}$ m

ν = KINEMATIC VISCOSITY

$\cong 10^{-6}\ \frac{m^2}{s}$

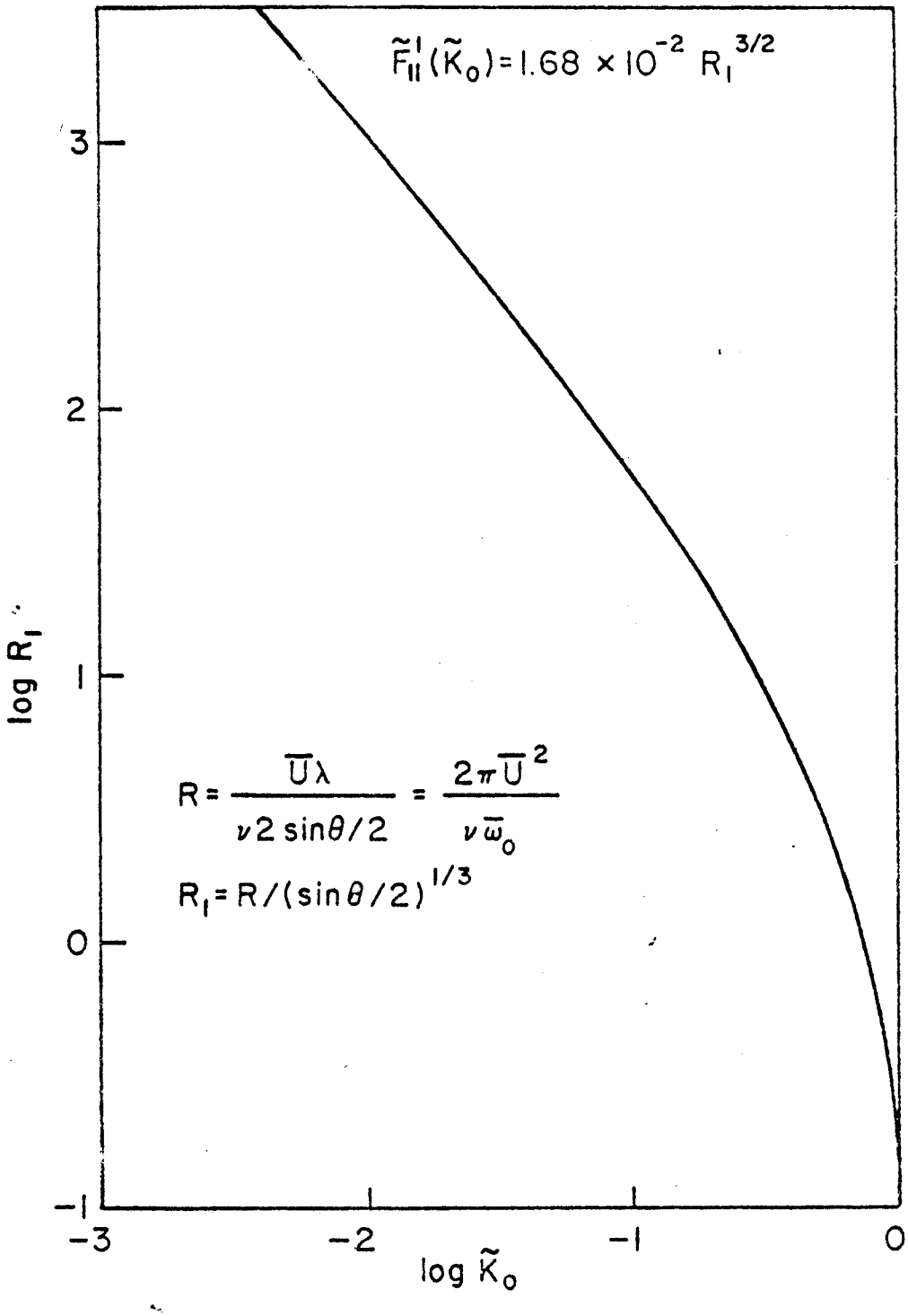

Fig. 4.4 Wavenumber of Unity Ambiguity to Turbulence Ratio under Optimum Conditions.

and the Kolmogrov microscale is given by

$$\eta = \left(\frac{\nu}{\varepsilon}\right)^{1/4} \tag{4.9}$$

where ε is the rate of dissipation of turbulence energy of which

$$\varepsilon = \frac{3}{2}\frac{d\overline{u^2}}{dt} \simeq \frac{u'^3}{\mathcal{L}_{11}} \tag{4.10}$$

typically $\frac{u'}{U} \simeq .15$ and

$$\mathcal{L}_{11} \simeq 0.06\,x \simeq 0.06\,D$$

where D = .076

in this case, ε can be estimated as

$$\varepsilon \simeq \frac{(2.07)^3}{0.0046}$$

$$\simeq 1940 \quad m^2/s$$

hence

$$\eta \simeq \left(\frac{10^{-18}}{1940}\right)^{1/4}$$

$$\simeq 4.76 \times 10^{-6} \quad m$$

First we compute the parameter R, which is just the Reynold's number based on the smallest length that can be resolved in the mean flow direction; since the laser light waves make an angle $\theta/2$ with the direction of the mean flow,

then $\frac{\lambda}{2\sin\frac{\theta}{2}}$ is the smallest length that can be resolved in that direction:

$$R = \frac{\bar{u}\,\lambda}{2v\sin\frac{\theta}{2}} \simeq \frac{(13.8)(633\times10^{-9})}{2(10^{-6})(0.063)}$$

$$\simeq 69 \qquad (4.11)$$

and

$$R_1 = \frac{R}{(\sin\frac{\theta}{2})^{1/3}}$$

$$\simeq 173.4 \qquad (4.12)$$

Since we are measuring the power spectrum, we have to obtain $\frac{m^2}{s}$ spectrum which we will call $N_{uu}(o)$. It is easier to work from equations (5.5.6) of George and Lumley who have already transformed the lowest spectral height of ambiguity to a dimensional wavenumber spectrum

$$\tilde{F}'_{11}(0) = 1.68\times10^{-2} R_1^{3/2}$$

$$\simeq 38.4 \qquad (4.13)$$

Again from equation (3.1.24) of George and Lumley, $\tilde{F}'_{11}(0)$ can be related to the true spectrum $F'_{11}(k)$ as

$$F'_{11}(k) = \varepsilon^{1/4}\nu^{5/4}\tilde{F}'_{11}(0)$$

$$= \frac{\nu^2}{\eta}\tilde{F}'_{11}(0) \qquad (4.14)$$

We now convert from the wavenumber spectrum to the power spectrum; i.e. from $\frac{m^3}{s^2}$ to $\frac{m^2}{s}$. The two spectra are related by

$$F_{11}'(k)\,dk = N_{uu}(f)\,df \tag{4.15}$$

which implies that

$$N_{uu}(0) \simeq \frac{2\pi}{\bar{u}} F_{11}'(k) \tag{4.16}$$

~~since~~

Substituting (4.9) and (4.10) into (4.11), we get

~~then~~ $$N_{uu}(0) = \frac{2\pi}{\bar{u}} \frac{\nu^2}{\eta} (1.68 \times 10^{-2} R_\lambda^{3/2})$$

$$= \frac{2\pi}{138} \frac{(10^{-6})^2}{4.76 \times 10^{-6}} (1.68 \times 10^{-2})(173.4)^{3/2}$$

$$= 3.64 \times 10^{-6} \tag{4.17}$$

The value of the turbulence spectrum at the origin is computed from Tennekes and Lumley

$$F(0) = \int_{-\infty}^{\infty} \overline{u'^2}\, \rho(z)\, dz = 2\overline{u'^2}\, \mathcal{I} \tag{4.18}$$

where $\mathcal{I} = \frac{\mathcal{L}_{11}}{\bar{u}}$ is the integral scale

For the jet mixing layer,

$$u' \simeq 0.15\,\bar{U}$$

$$\ell_{11} \simeq 0.06x \simeq 0.06D \simeq 4.56\times10^{-3}\ m$$

therefore

$$F(0) = 2(2.07)^2\,\frac{(4.56\times10^{-3})}{13.8}$$

$$\simeq 2.83\times10^{-3}\ \ m^2/\text{Hz} \qquad (4.19)$$

The spectral breakpoint is also given by Tennekes and Lumley as occurring at

$$\frac{0.1}{T} \simeq \frac{(0.1)(13.8)}{4.56\times10^{-3}}$$

$$\simeq 300\ \ \text{Hz} \qquad (4.20)$$

We can begin constructing the spectrum by utilizing the results from (4.12), (4.14), and (4.15), as shown in Fig. 4.5. Consequently, f_{LP} can be easily identified at about 18 KHZ.

With Disa 55N20 frequency tracker, the highest low pass filter setting is about 19 KHZ, thus this is the frequency we would use to estimate the contribution of phase fluctuation based on equation (4.8).

$$\overline{w'^2}_{meas} \simeq [\,(0.15\bar{U})\,E\,]^2$$

$$\simeq [\,(0.45)(13.8)(0.2\times10^{-6})\,]^2$$

$$\simeq 1.7\times10^{-11}\ \ \text{Hz}$$

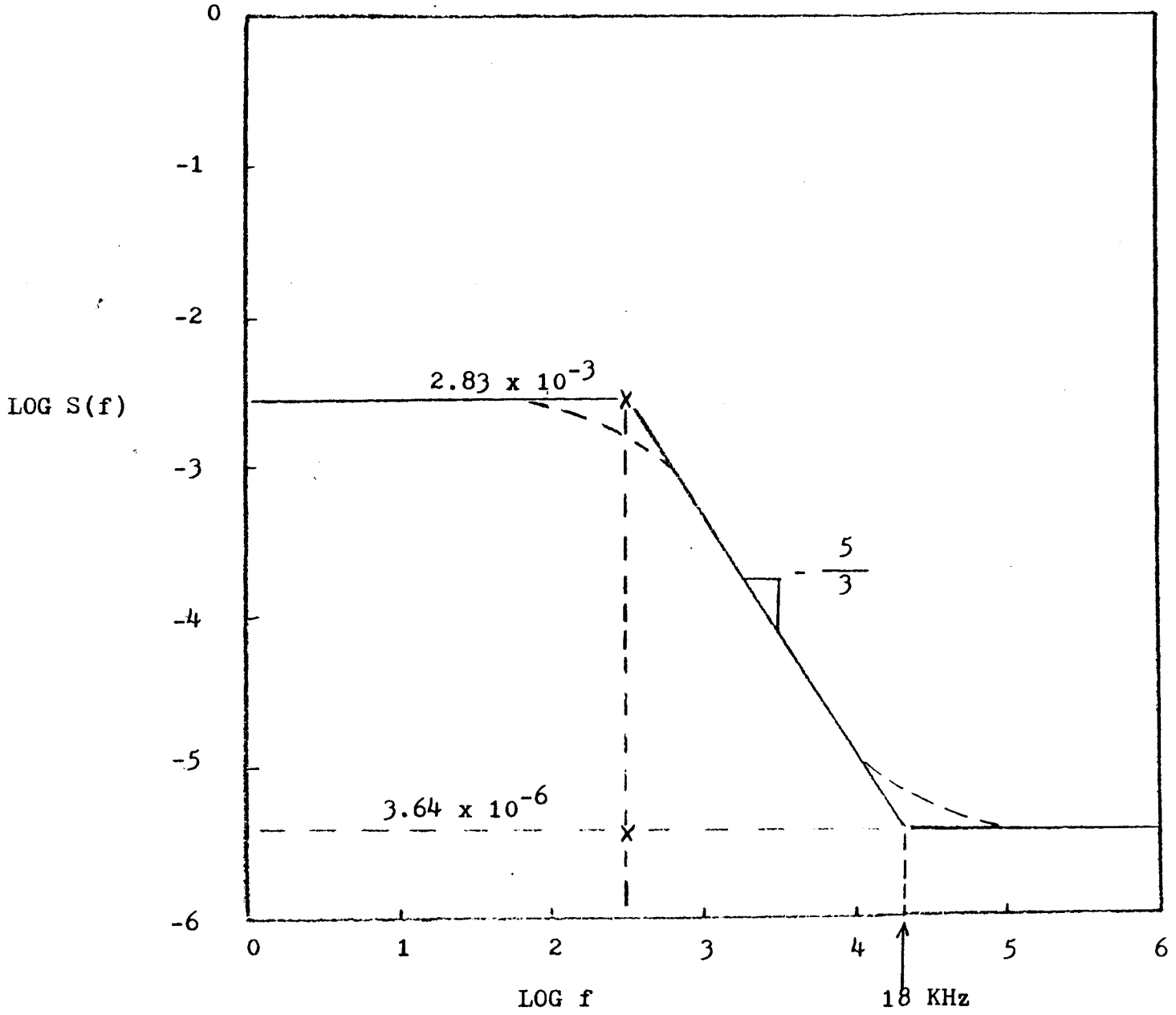

Fig. 4.5 Computational estimate of the velocity & ambiguity spectra for this experiment

and

$$\overline{\phi^2} \simeq 45.64 f_{cp}^2$$

$$\simeq 1.6 \times 10^{10} \text{ Hz}$$

therefore

$$\frac{\overline{\phi^2}}{\overline{\omega'^2_{meas}}} \simeq 9 \times 10^{-2} \qquad (4.21)$$

Clearly, with the result of (4.21), we can confidently believe that the contamination of Doppler ambiguity is well within the range of any experimental error.

CHAPTER 5

SIGNAL DROPOUT ANALYSIS

The common problem of LDA analog processing with multiple particles in the measuring volume is the signal dropout. The physical reasonS for the signal dropout are as follows:

1) The signal amplitude is too low due to:
   (a) Poor S/N ratio.
   (b) Too few and too small scattering particles.
   (c) Phase cancellation among the particles.
2) The particle transit time is much too short relative to the loop response time of the tracking type processor.
3) There are no particles inside the measuring volume at all.

In the case of using the frequency tracker with phase-lock loop design, the loss of tracking signal occurs when the input signal is lower than the preset threshold level, or the slew rate or capture range limit is exceeded. How the tracker processes the signal at the time of dropout influences the statistical parameters in the flow. It is critical to select a compensation scheme to preserve those

statistical quantities (i.e. mean, mean square, moment, and spectrum) as dropout occurs.

Buchhave et al (1979) proposed modelling the lock signal by an indicator function, I(t),. When the tracker is in lock I(t) = 1 and when dropout is present, I(t) = 0. Using this the tracker output can be represented as

$$\tilde{f}(t) = f(t) \cdot I(t) \qquad (5.1)$$

where $\tilde{f}(t)$ is the instantaneous tracker output, and f(t) is signal being sampled by the tracker (i.e. no dropout).

Buchhave et al. (1979) analyzed three possible ways of handling the tracker output at dropout time and concluded that holding the last value prior to dropout was the preferred method if the dropout time was small compared to the turbulence integral scale. Essentially, the tracker output is:

$$\tilde{f}(t) = f(t)\, I(t) + \hat{f}(t)\,[\,1 - I(t)\,] \qquad (5.2)$$

where

$$\hat{f}(t) = f(t_k), \text{ for } t_k \le t \le t_{k+1}$$

t_k ($k = 1, 2, 3, \ldots$) is the drop-out

The means can be shown to be given by

$$\overline{\tilde{f}} = \overline{f}\,\overline{I} + \overline{\hat{f}}\,(1 - \overline{I})$$

$$= \overline{f} \qquad (5.3)$$

where the overbar is the usual ensemble average.

In fact,

$$\overline{\tilde{f}^n} = \overline{f^n}$$

for all n. The fluctuating quantities can also be calculated as

$$\overline{f'} = \left(\overline{f^2} - \overline{f}^2\right)^{1/2} \qquad (5.4)$$

The conclusion is that if the dropout duration is smaller than the integral scale and the tracker holds the last value, all the moments of velocity are conserved.

The important assumption on which the above statement is based is that the dropout of the signal must be statistically independent of the velocity of the fluid. In the present investigation the validity of this assumption is investigated. We will propose a computational algorithm to obtain the correlation coefficient of the dropout and flow velocity. The digital outputs from the Disa 55N20 tracker yield both the Doppler frequency and lock indication. These were utilized with a Disa 55G20 buffer interface and minicomputer to perform data acquisition and real time analysis.

The digital indication of the frequency from Disa 55N20

frequency tracker is obtained inside the tracker by counting the sinusoidal output of the VCO at regular intervals, the counting occurs over a time period, T_G , equal in value to 128 divided by the maximum range setting of the tracker. The digital output is $D = 256 \frac{f_T}{RANGE}$ where f_T is the tracker frequency and the range is the maximum tracking frequency for the selected range. The D is an eight bit digital representation given by $D = D_7 D_6 D_5 D_4 D_3 D_2 D_1 D_0$. The D value is actually the average value of the tracker frequency ($= f_{VCO}$) over the counting period. The sampling frequency is fixed for each tracking range. In the case of present work, T_S , the sampling frequency in the range of 1-10 MHZ, is equal to $14. \pm 0.1$

The computed D is read out to the buffer output with a negative data ready ($\overline{DR}$) pulse. However, the readout of the D value is valid only when the calculation of D takes place at a point where the signal quality is satisfactory and there is no dropout. The lock detection will generate a $\overline{Lock}$ signal which is either 0 or 1 ($\overline{Lock}$=1 is out of lock). This lock output is simultaneously available at the output buffer with the frequency signal. Therefore the lock signal indicates whether the D output is legitimate or not. It should be emphasized that the $\overline{DR}$ pulse is output after each calculation of D regardless of the result of the calculation. If $\overline{Lock}$ is one, the D output will be latched

on the last computed value until $\overline{\text{Lock}}$ is zero again.

The channel for the digital out is at the rear panel of the tracker. A 40 pole flat cable connects the output channel to the interface's multiplexer input.

In order to take the advantage of the tracker's digital output, the tracker was interfaced through the Disa 535G20 buffer interface to a DEC PDP 11/03 minicomputer by parallel transmission. This computer data acquisition set-up is shown in Fig. 5.1. The buffer interface is consisted of five parts. The main frame provides the power and the backplane. An output demultiplexer and input multiplexer take care of all the input and output functions. There is a logic control board which handles priority of the incoming data and labels each peice of data as what it is representing. All the incoming data are then transmitted to the buffer memoryy control board where data are transiently stored in the 512 words silo type memory and then transmitted to the computer interface unit at the maximum rate the computer can handle.

This buffer interface was designed to accept asynchronous data with a throughput rate of 1 microsecond. The reason why such a unit is desired is because in most LDA measurements the data rate of the processor exceeds the

TRACKER PROGRAM FLOW-CHART

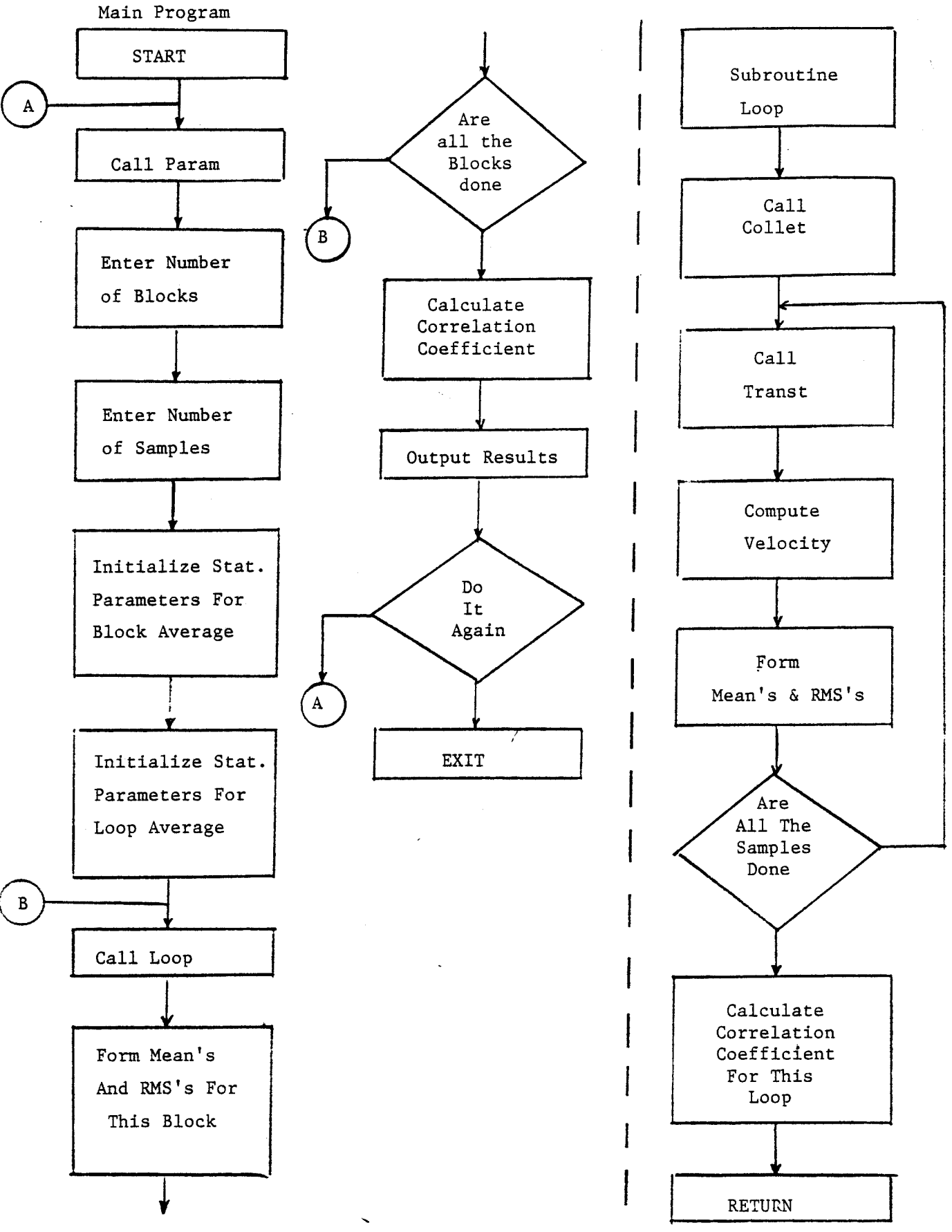

capability of most mini or micro computers for continuous data acquisition without any loss. Although the data can temporarilyy reside in the buffer memory, there is only a limited space available. In case the data rate is extremely high there is a possibility of overflow, with the result that some of the data would be lost. In order to caution the user of such occurance, the control logic board will tag a bit in the transmitted data word to in- dicate buffer memory overflow. During our investigation, this bit is always checked to insure no loss of data. In these experiments, we were able to collect 5000 samples for each batch without triggering buffer overflow. Consequently, this was the maximum number of samples allowed in the data collection software.

The correlation coefficient algorithm is derived as follows:

Let

u(t) = instantaneous value of Doppler frequency

I(t) = instantaneous value of lock indication

With these two quantities available, we can use ensemble average to compute the fluctuating components

$$u' = u - \bar{u}$$

$$i = I - \bar{I}$$

Then the correlation coefficient of u' and i is

$$\text{CORR. COEFF} = \frac{\overline{u'i'}}{\sqrt{\overline{u'^2}}\sqrt{\overline{i'^2}}} \qquad (5.7)$$

The averages can be formed as

$$\overline{u'i'} = \overline{(I-\bar{I})(u-\bar{u})} = \overline{Iu} - \bar{I}\bar{u} \qquad (5.8)$$

$$\overline{u'} = \sqrt{\overline{u'^2}} = \left[\overline{(u-\bar{u})^2}\right]^{1/2}$$

$$= (\overline{u^2} - \bar{u}^2)^{1/2} \qquad (5.9)$$

$$\overline{i'} = \sqrt{\overline{i'^2}} = \left[\overline{(I-\bar{I})^2}\right]^{1/2}, \text{ SINCE } \overline{I^2} = \bar{I}$$

Therefore $$= \left[\bar{I}(1-\bar{I})\right]^{1/2} \qquad (5.10)$$

$$\text{CORR. COEFF} = \frac{\overline{u'i'} - \bar{u}'\bar{i}'}{\left[\bar{I}(1-\bar{I})\right]^{1/2}\left[\overline{(u-\bar{u})^2}\right]^{1/2}}$$

There are two different conditional averaging techniques applied to compare the difference between the weighted and unweighted functions:

(1) The mean and rms values representing only locked data.

If tracker is out of lock, the samples taken will be discarded.

$$\bar{u}_{ABS} = \frac{\sum_{j=1}^{N} u_j I_j}{\sum_{j=1}^{N} I_j} \qquad (5.12)$$

$$\overline{u^2}_{ABS} = \frac{\sum_{j=1}^{N} u_j^2 I_j}{\sum_{j=1}^{N} I_j} \qquad (5.13)$$

$$\overline{u'}_{ABS} = (\overline{u^2}_{ABS} - \bar{u}_{ABS}^2)^{1/2} \qquad (5.14)$$

(2) Weighted mean and rms values.

If tracker is out of lock, the present value will take on the value of the previous sample.

$$\overline{u}_{WT} = \frac{\sum_{j=1}^{N} u_j I_j + u_{j-1}(1-I_j)}{N} \qquad (5.15)$$

$$\overline{u^2}_{WT} = \frac{\sum_{j=1}^{N} [u_j I_j + u_{j-1}(1-I_j)]^2}{N} \qquad (5.16)$$

$$\overline{I} = \frac{\sum_{j=1}^{N} I_j}{N} \qquad (5.17)$$

$$\overline{C} = \frac{\sum_{j=1}^{N} I_j u_j}{N} \qquad (5.18)$$

$$\sqrt{\overline{u^2}_{WT}} = (\overline{u^2}_{WT} - \overline{u}^2_{WT})^{1/2} \qquad (5.19)$$

$$\sqrt{\overline{I^2}_{WT}} = [\overline{I}(1-\overline{I})]^{1/2} \qquad (5.20)$$

$$(\text{CORR. COEFF})_{WT} = \frac{\overline{C} - \overline{I}\,\overline{u}_{WT}}{\sqrt{\overline{u^2}_{WT}}\sqrt{\overline{I^2}_{WT}}} \qquad (5.21)$$

The flow chart of the program is shown in Fig. 5.2. Total batch averaging is applied after each individual batch is completed.

There are a number of subroutines written in assembly language to perform basic interfacing functions. The subroutine PARAM sets the bandwidth and tracker range remotely, COLLECT establishes the static control words for the buffer interface to collect the data via interrupt technique and transmit the acquired data via DRV-11 parallel interface to the computer. The data are then taken out of preassigned memory location one at a time to be converted from internal compressed format to floating point format by the subroutine TRANSF. All these subroutines are linked to

a main program which ultimately carries out the computational algorithm to get the correlation coefficient. The complete listing of all the software designed for this purpose is in the Appendix.

After the algorithm was formulated in the software, we needed to check the validity of it. Two methods were used. One used a simulated input signal which corresponded to a known result. The other method tested the program with an actual jet flow at two different velocities.

The arrangement of the first test is illustrated in Fig. 5.2. The idea is to generate a FM modulated signal which simulates a series of Doppler bursts that yield 50% of the signal in dropout and the other 50% in lock. This simple test ran very well. The result showed $\bar{I}(t) = .499$ and a correlation coefficient = .951. The slight imperfection in the data can be attributed to the computer truncation error.

The second test was conducted on a small jet which has a construction similar to the one used in the flow measurement section. This jet has a diameter of 5.4 cm. The location of measurement is three diameters down- stream in the center of the mixing layer. The first run was at an exit velocity of 4 m/s and the second run was at 7.6 m/s.

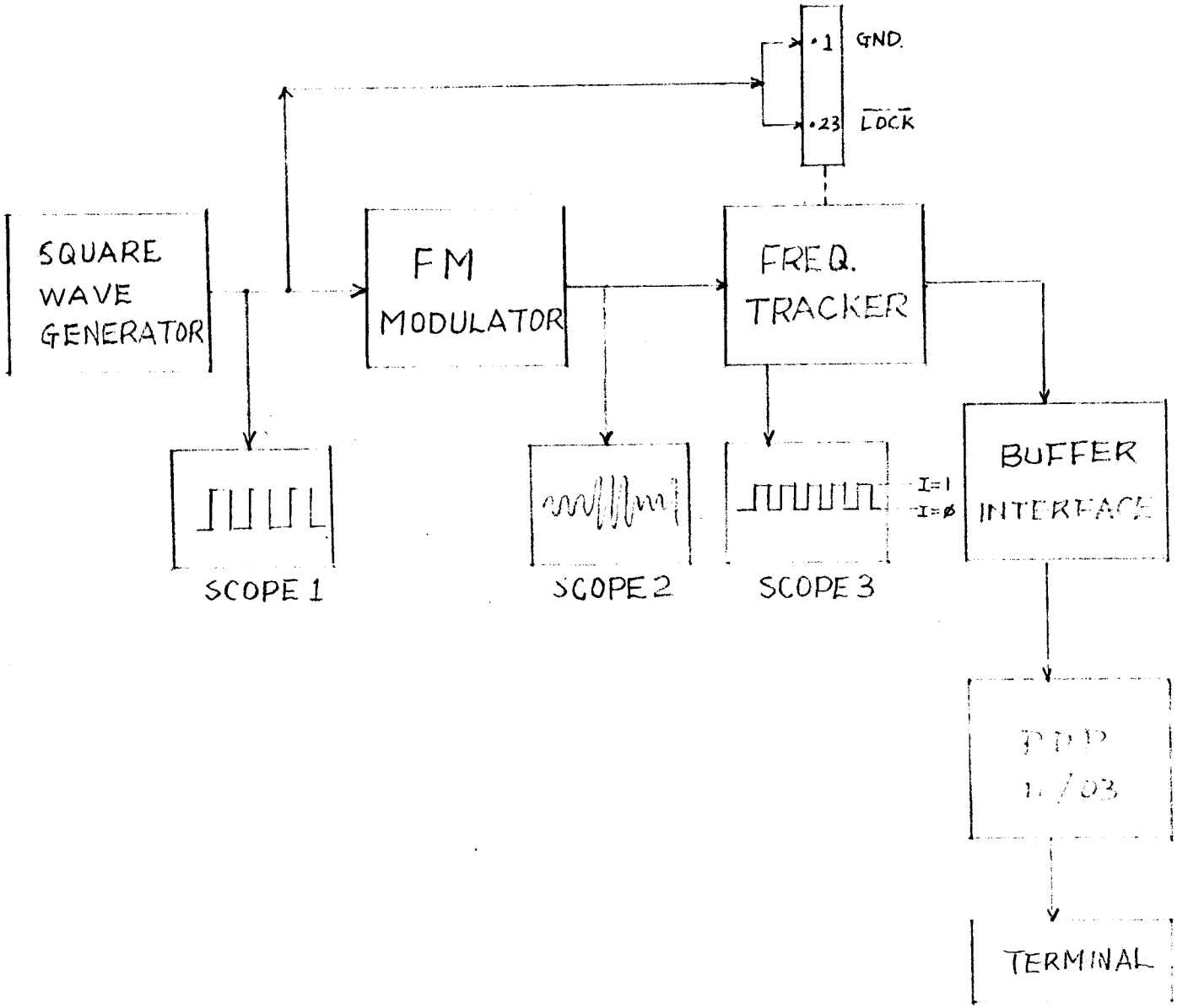

Fig. 5.2 Block diagram of the first test for the Tracker program

Both results are shown in Table 5.1 and 5.2. It is evident that the correlation coefficients for both velocities are low; thus there is only very weak correlation relation between velocity and dropout. However, the dropout seems to correlate with the turbulence intensity. The RMS frequency of the higher velocity run is almost double that of the lower velocity run, and correspondenly, the mean-lock is about half.

The results obtained for absolute averaging and weighted averaging do not show significant deviation from each other, thus the simpler algorithm can be used since less computational complexity is involved. In spite of the fact the dropout and turbulence are correlated, this correlation does not appear toaffect the validity of the assumptions used in the dropout analysis.

SQUARE WAVE GENERATOR SETTING:

FREQUENCY= 1 KHz

FM MODULATOR SETTING:

FREQUENCY= 5 MHz

FM MODULATION FREQUENCY= 1 KHz

FREQUENCY TRACKER SETTING:

RANGE= 10 MHz

LOW PASS FILTER= 19.4 KHz

MEAN VELOCITY COMPUTER READ-OUT= 3.74 MHz

EXPECTED RESULTS:

MEAN LOCK= 0.5

CORRELATION COEFFICIENT= ± 1

ACTUAL COMPUTER OUTPUT:

MEAN LOCK= 0.499

CORRELATION COEFFICIENT= -0.950

MEAN FREQUENCY= 3.743 MHz

Table 5.1 Result of the first test of the Tracker program

FREQUENCY TRACKER SETTINGS:

LOW PASS FILTER= 19.4 KHz

TRACKER RANGE= 10 MHz

MEASURING LOCATION:

X/D= 3, r/R= 1

NUMBER OF DATA PER BATCH: 5000

NUMBER OF BATCH: 15

COMPUTER OUTPUT FOR TWO DIFFERENT EXIT VELOCITIES

EXIT VELOCITY(m/s):	11	13
MEAN VELOCITY(m/s):	6.7	7.9
RMS VELOCITY(m/s):	1.3	2.1
MEAN LOCK:	0.97	0.52
CORR. COEFF.:	2.6×10^{-2}	1.3×10^{-1}
TURBULENCE INTENSITY:		
$u'/\bar{U}$	19 %	27 %
u'/U_E	12 %	16 %

Table 5.2 Result of the second test of the Tracker program

CHAPTER 6

MIXING LAYER DATA ANALYSIS

Measurements across the mixing layer were recorded at x/D = 1,2,3 and 4. The tracker outputs were connected to the DC and RMS voltmeters. A 100 second of integration time constant was selected to ensure convergence of time averaged signal. The error due to finite integration time can be estimated from Tennekes and Lumley (1972). The finite time average is given by

$$u_T = \frac{1}{T} \int_{t_o}^{t_o+T} \tilde{u}(t)\, dt \qquad (6.1)$$

where T is the integration time constant, and $\tilde{u}(t)$ is the instantaneous signal. If $t_o = 0$, the difference between u_T and the true mean value $\bar{u}$ is given by

$$u_T - \bar{u} = \frac{1}{T} \int_o^T [\tilde{u}(t) - \bar{u}]\, dt$$

$$= \frac{1}{T} \int_o^T u'(t)\, dt \qquad (6.2)$$

Now the mean square error can be estimated by

$$\overline{(u_T - \bar{u})^2} \simeq \frac{2\,\overline{u'^2}\,J}{T} \qquad (6.3)$$

The integral scale velocities of the mixing layer can be

estimated from the results cited in Chapter 4 at X/D =1, $\mathcal{T} \simeq$ 3.3x10 seconds and the fluctuating velocity u'$\simeq$2.1 m/s from which the relative error can be calculated to be less than 0.4%. The mean and rms velocity profiles are shown in Fig. 6.1a-d. The mean velocities are normalized by the jet exit velocity, $\frac{\bar{u}}{\bar{u}_E}$; and the radial distances by the axial distance, $\frac{r-R}{x}$. This is shown in Fig. 6.2A. The profiles are locally self similar. This is because the mixing layer is sufficiently thin that the radial spreading can be neglected and a 2-dimensional flow approximations is appropriate. This indicates that the jet mixing layer is not fully developed at one diameter downstream. Since the rest of the profiles exhibit self-similarity, it is clear that the jet must achieve self similarity between x/D = 1 and 2.

The LDA data are checked with the results obtained by Khwaja (1980) in which hot wire data were taken in the mixing layer of an axisymmetric air jet and compared with various authors. Fig. 6.2b shows how LDA data compares to the well established hot wire data.

The momentum flux at the exit plane can be expressed as

$$M_o = \pi \bar{u}_E^2 \frac{D^2}{4} \qquad (6.4)$$

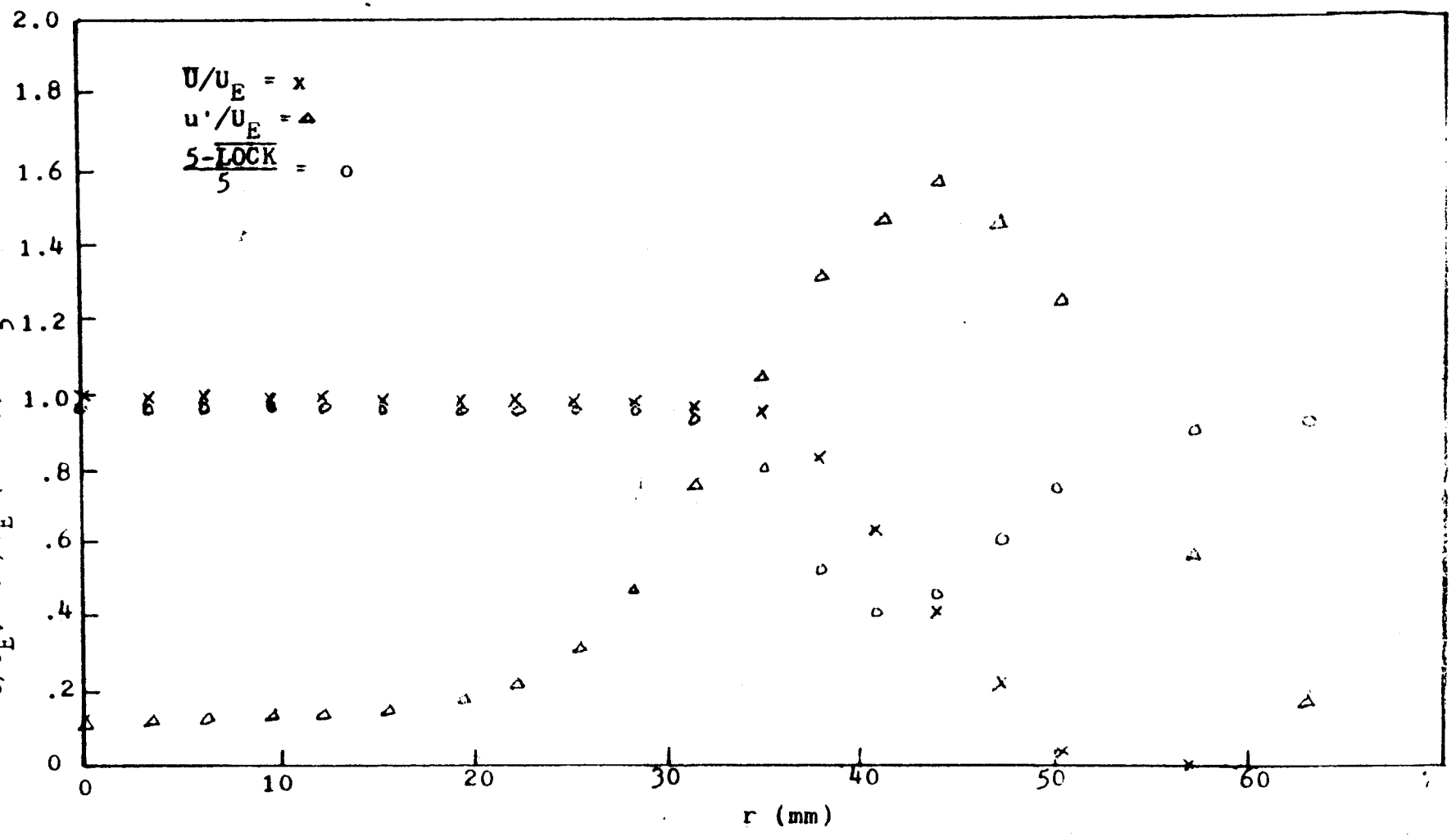

Figure 6.1a Nondimensional mean, fluctuating velocities, and drop-out data for X/D=1

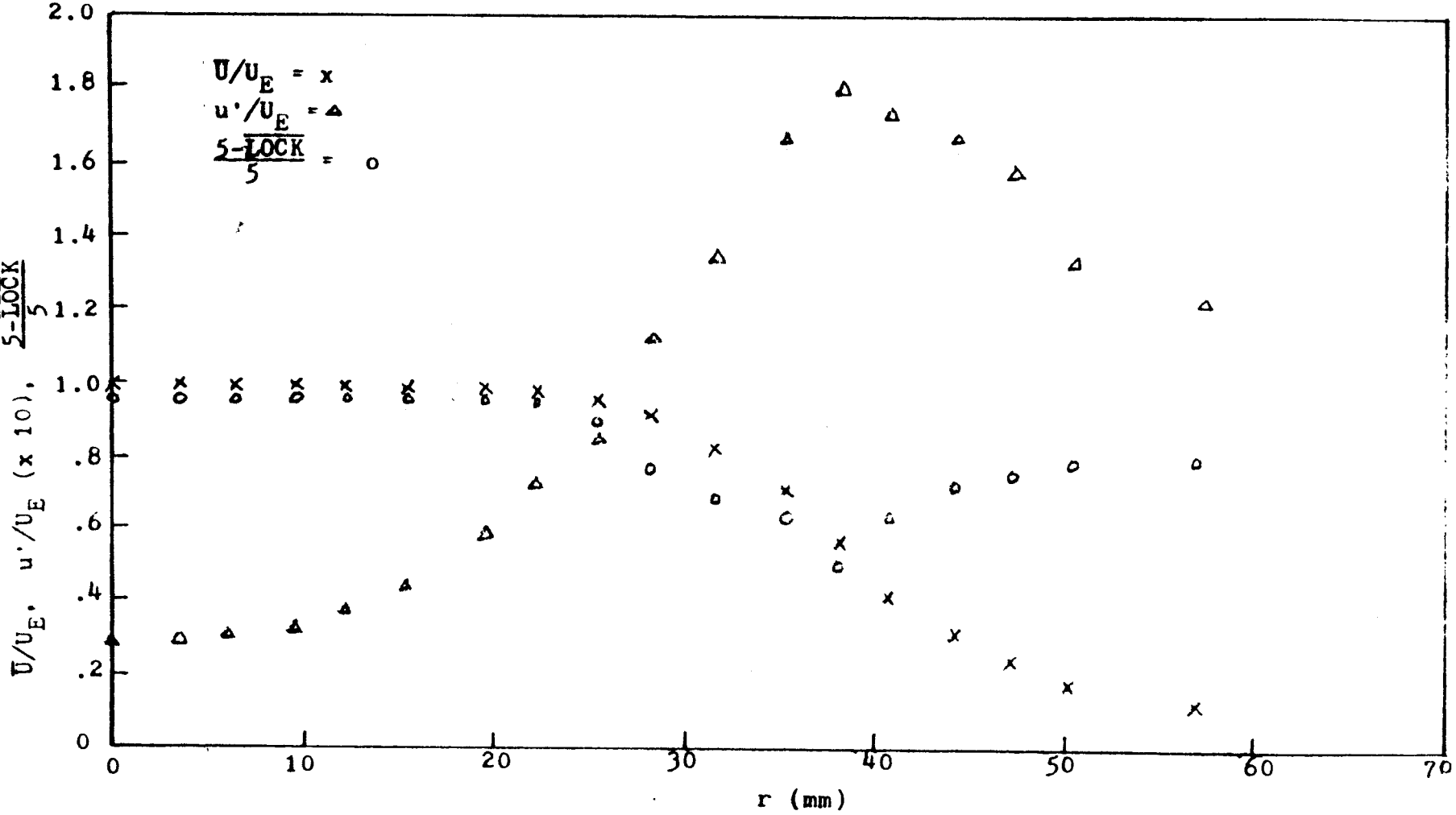

Figure 6.1 b Nondimensional mean, fluctuating velocities, and drop-out data for X/D= 2

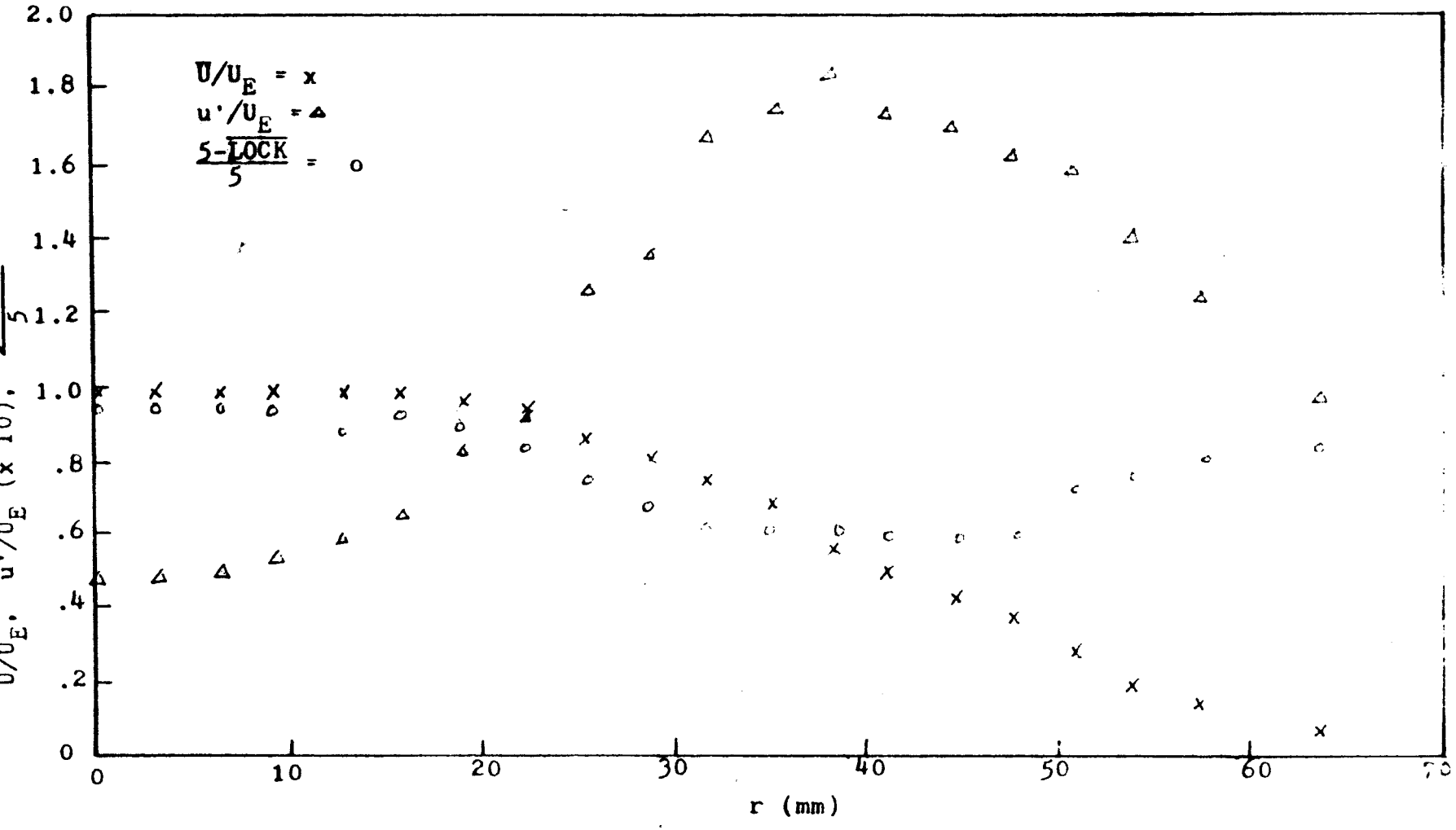

Figure 6.1C Nondimensional mean, fluctuating velocities, and drop-out data for X/D=3

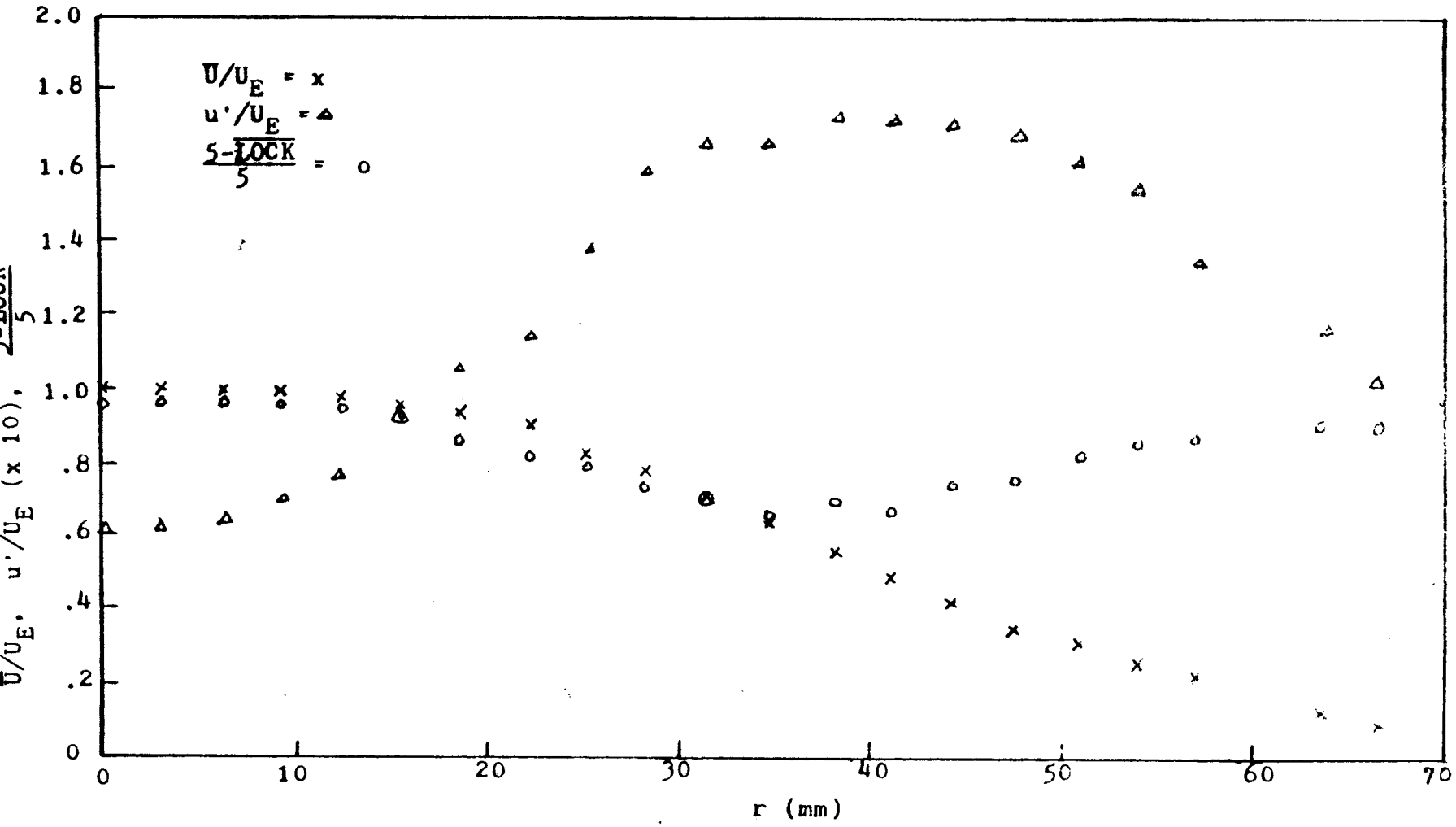

Figure 6.1 d Nondimensional mean, fluctuating velocities, and drop-out data for X/D= 4

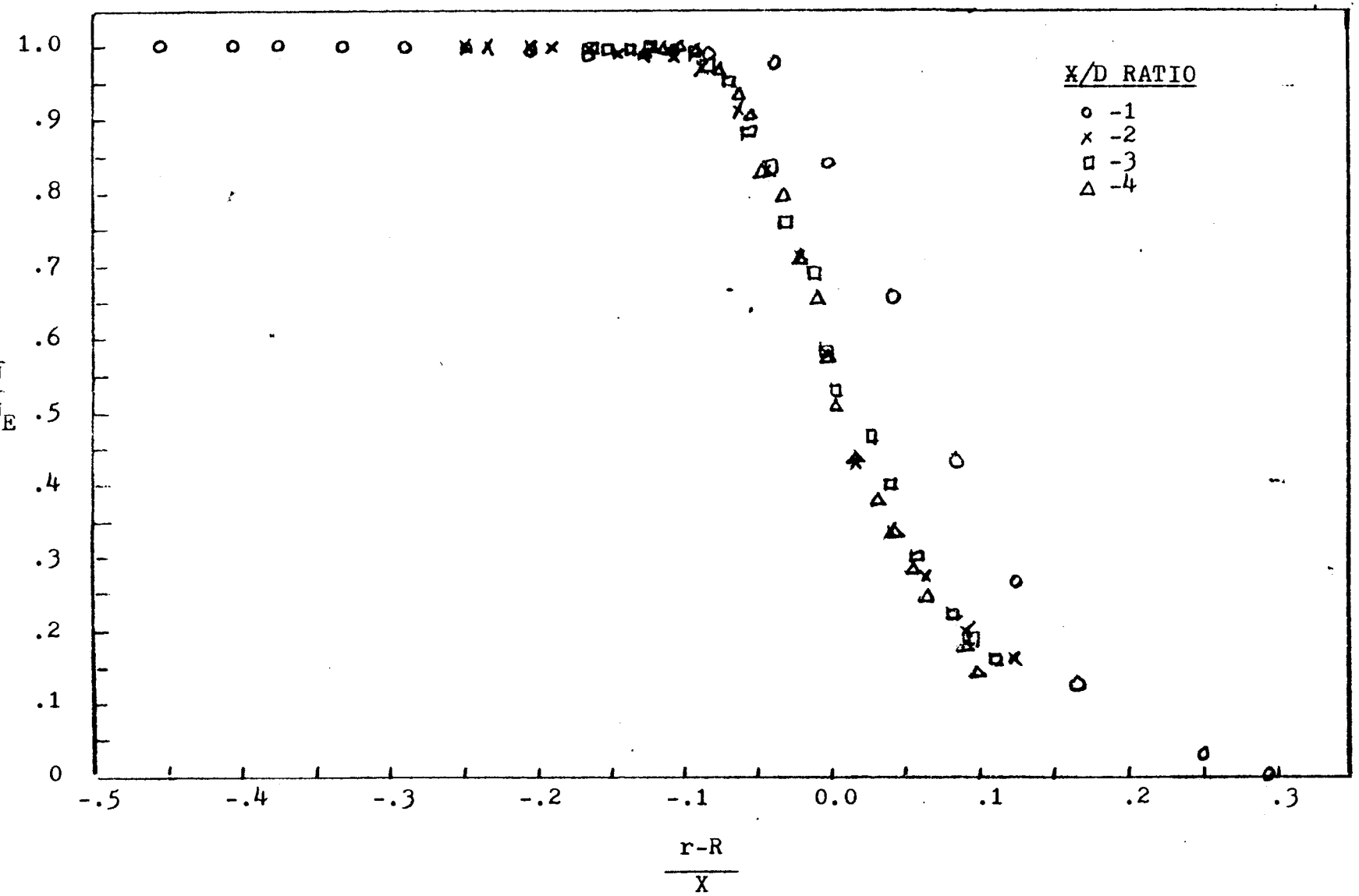

Fig. 6.2a Self-similarity mean velocity profile

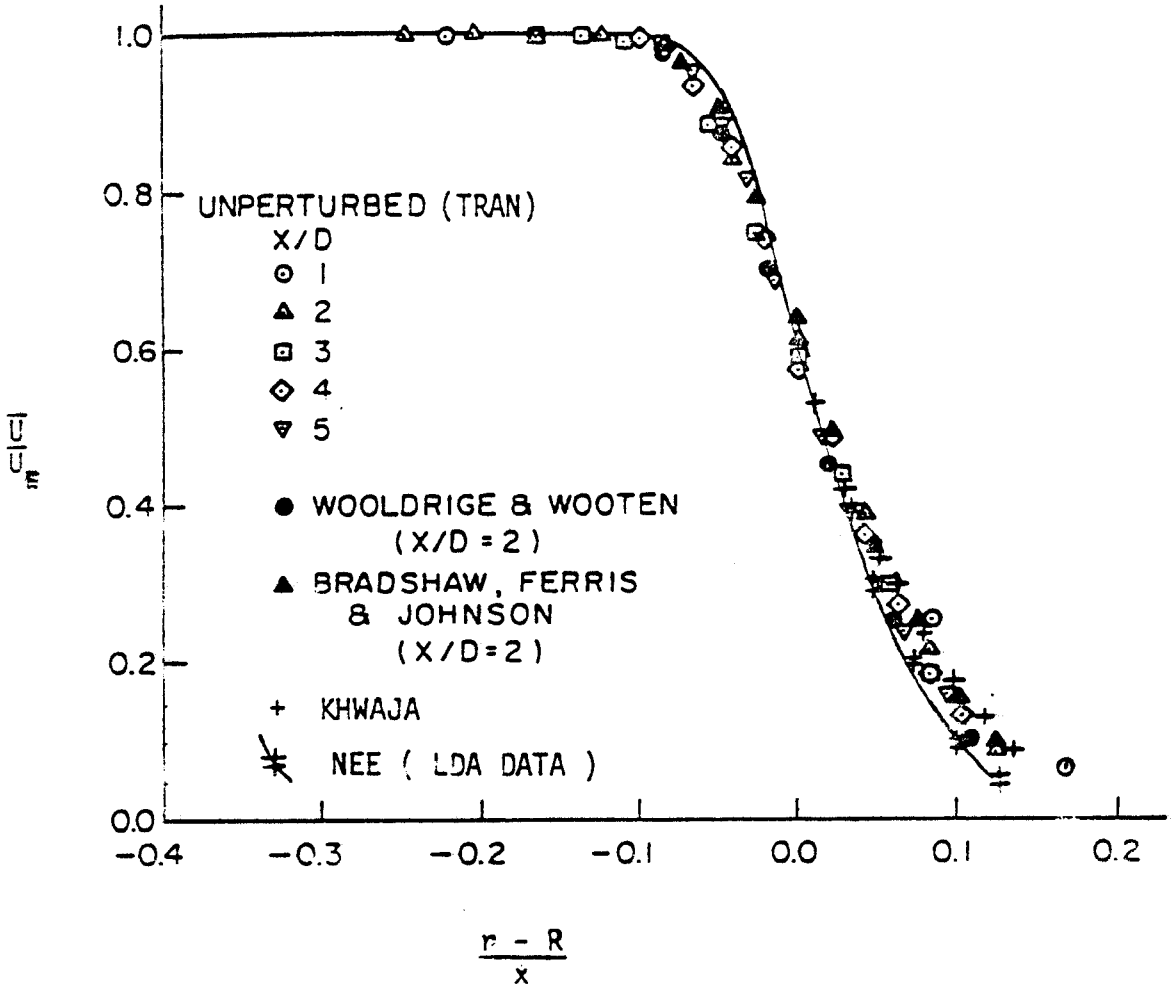

FIG 6.2b Comparison of Hot-Wire & LDA data.

and at any other downstream locations as

$$M_x = 2\pi \int_0^\infty \bar{u}^2 r\, dr \qquad (6.5)$$

since there are no other forces impulsed on the jet, the laws of physics require that momentum be conserved, meaning Mx = Mo. We can rewrite equation (6.5) in an expanded form as follows

$$M_x = 2\pi \overline{u_\ell}^2 \int_0^\infty \left(\frac{\bar{u}}{\overline{u_\ell}}\right)^2 r\, dr$$

$$= 2\pi \overline{u_\ell}^2 \frac{D^2}{4} \int_0^\infty \left(\frac{\bar{u}}{\overline{u_\ell}}\right)^2 \left(\frac{r}{\frac{D}{2}}\right) \left(\frac{dr}{\frac{D}{2}}\right) \qquad (6.6)$$

where $\bar{u}_\ell$ = center line near velocity. Thus by equating equ. (6.4) to (6.6), we get

$$\int_0^\infty \left(\frac{\bar{u}}{\overline{u_\ell}}\right)^2 \left(\frac{r}{\frac{D}{2}}\right) d\left(\frac{r}{\frac{D}{2}}\right) = \frac{1}{2}$$

We can plot $\left(\frac{\bar{u}}{\overline{u_\ell}}\right)^2 \left(\frac{r}{\frac{D}{2}}\right)$ against $\left(\frac{r}{\frac{D}{2}}\right)$ for x/D = 2,3, and 4, thereafter simply counting the area under the curve we can check it tosee if it is about 0.5. These plots are shown in Fig. 6.3, 6.4, and 6.5. Table 6.1 summarizes the result of momentum conservation check.

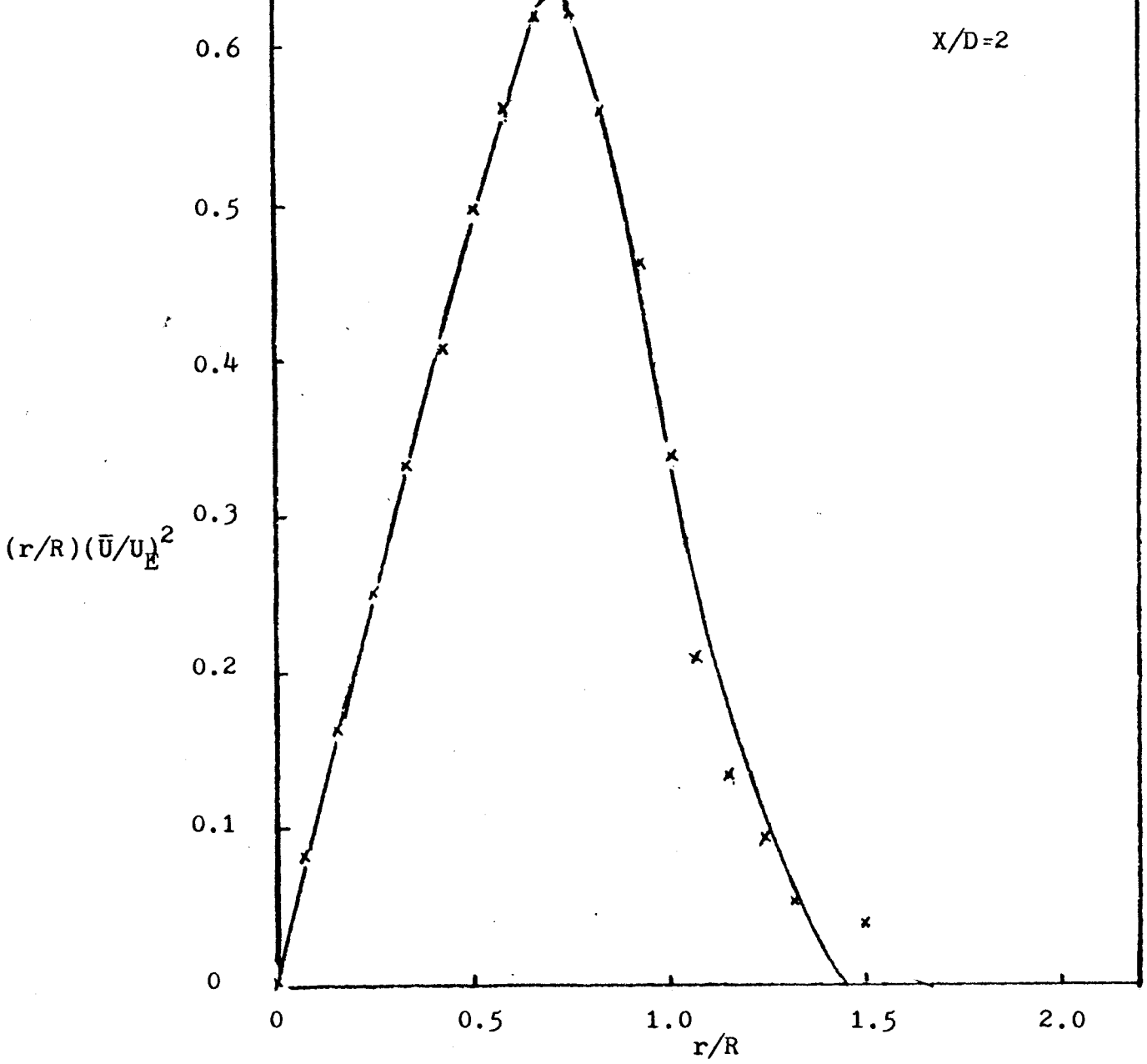

Fig. 6.3 Momentum conservation profile for X/D=2

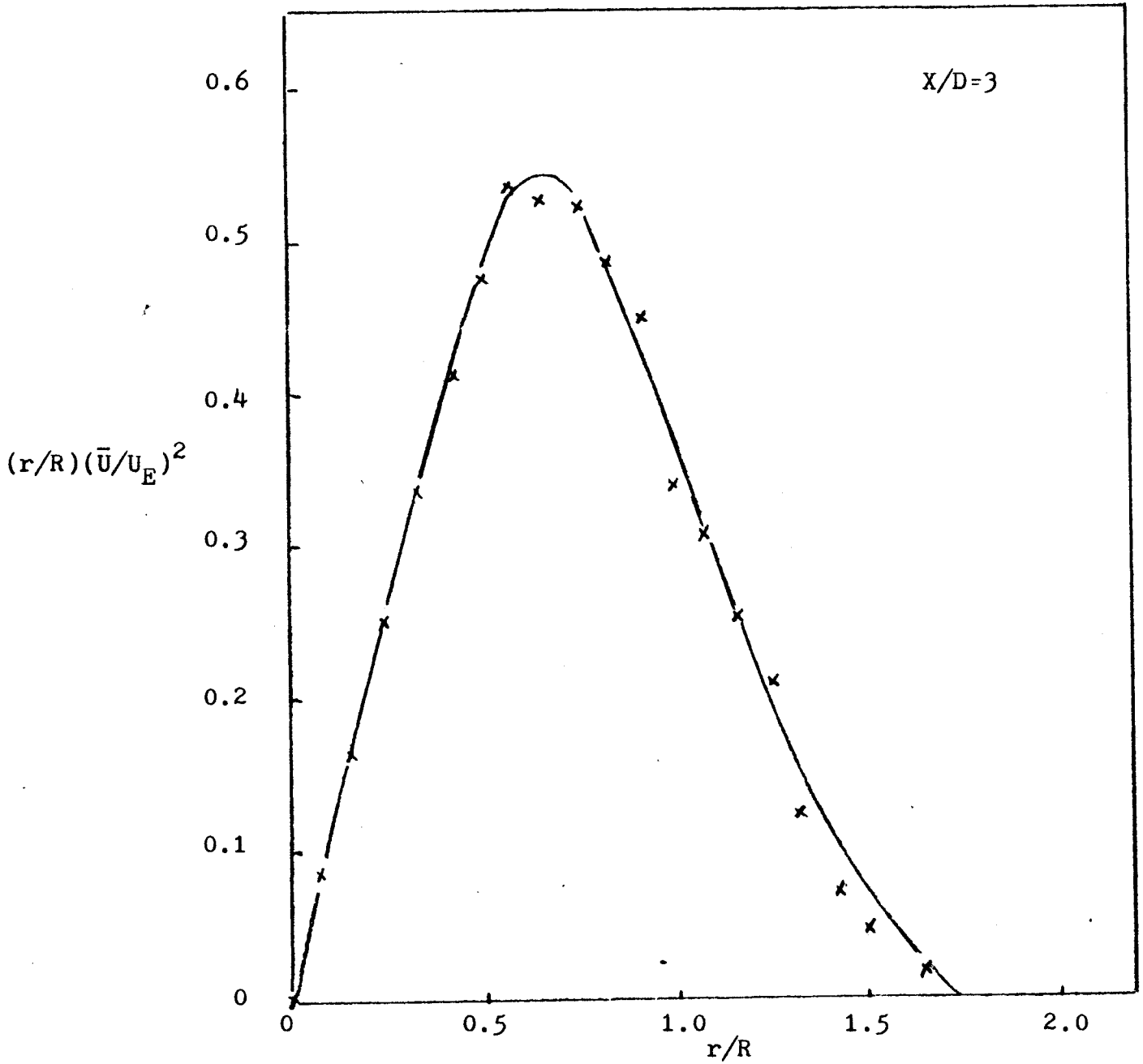

Fig. 6.4 Momentum conservation profile for X/D=3

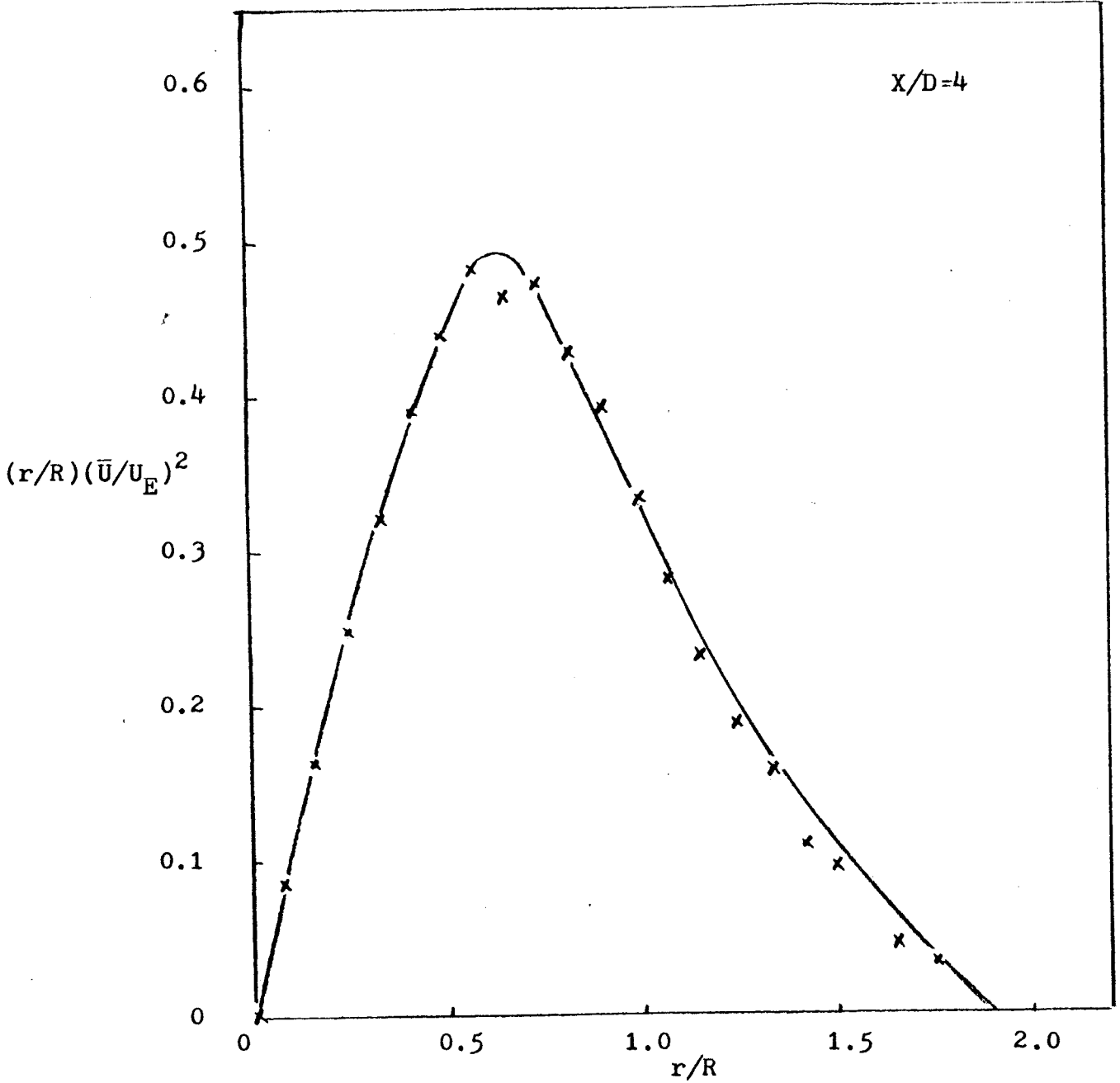

Fig. 6.5 Momentum conservation profile for X/D=4

X/D	Momentum
2	0.92
3	0.94
4	0.92

Table 6.1

The measurements appear to conserve momentum to within 92-94%. This is consistent with 6-8% momentum being carried by the turbulence.

An intriguing aspect of the jet is the entrainment of the surrounding fluid. Its existence is implied by the equation of Continuity:

$$\frac{\partial \bar{u}}{\partial x} + \frac{1}{r}\frac{\partial}{\partial r} rV = 0 \qquad (6.7)$$

rV represents the volumetric entrainment rate at a point, if we integrate the entire equation (6.7) and rearrange the terms

$$\int_0^r \frac{\partial r' V}{\partial r} dr' = -\int_0^r r' \frac{\partial \bar{u}}{\partial x} dr' \qquad (6.8)$$

then it is apparent that

$$(r\bar{V})_\infty - (rV)_0 = -\frac{d}{dx}\int_0^\infty r'\bar{u}(r')dr' \qquad (6.9)$$

since

$$rV\Big|_{r=0} = 0$$

The integral term of the above equation can be computed by plotting $\frac{r}{R}\left(\frac{\bar{u}}{u_\epsilon}\right)$ against $\frac{r}{R}$. These are shown in Fig. 6.6, 6.7 and 6.8. Again we can obtain the area under the curve by counting the boxes. The results are summarized in Table 6.2.

X/D	Entrainment integral
2	0.644
3	0.711
4	0.787

Table 6.2

When the integrals plotted against x/D in Fig. 6.9, the results fall on a straight line with a slope of 0.069 and intercept of 0.5. The value of 1/2 at the origin is consistent with the top hat profile at the exit. The linear dependence of the integral on X/D implies that the entrainment rate is constant over the range in which measurements were taken.

Since

$$\int_0^\infty \left(\frac{r}{R}\right)\left(\frac{\bar{u}}{u_\epsilon}\right)\frac{dr}{R} \simeq 0.5 + 0.069\,\frac{x}{D} \qquad (6.16)$$

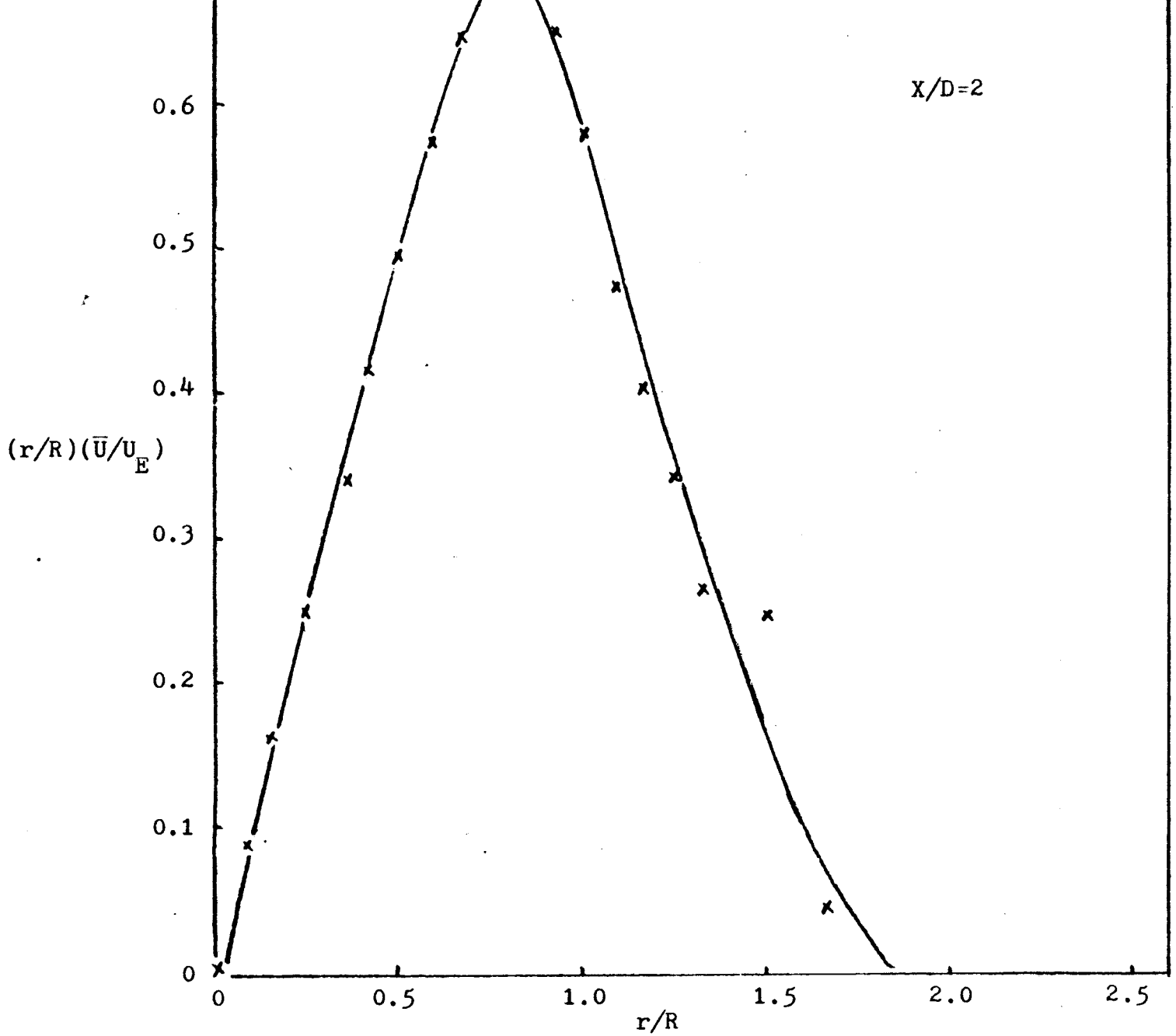

Fig. 6.6 Mixing layer entrainment profile for X/D=2

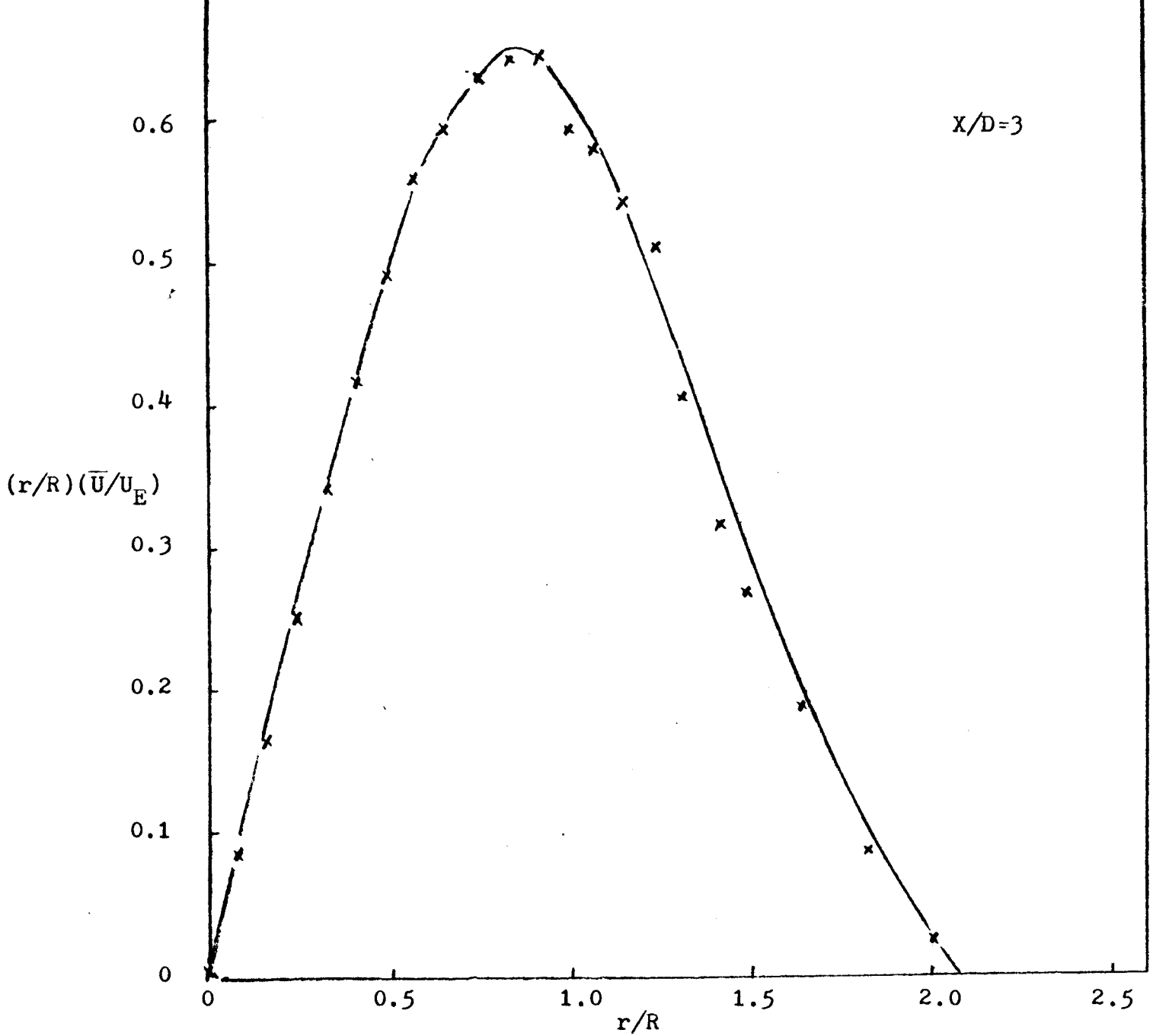
X/D=3
(r/R)(Ū/U_E)
0
0.1
0.2
0.3
0.4
0.5
0.6
0
0.5
1.0
1.5
2.0
2.5
r/R

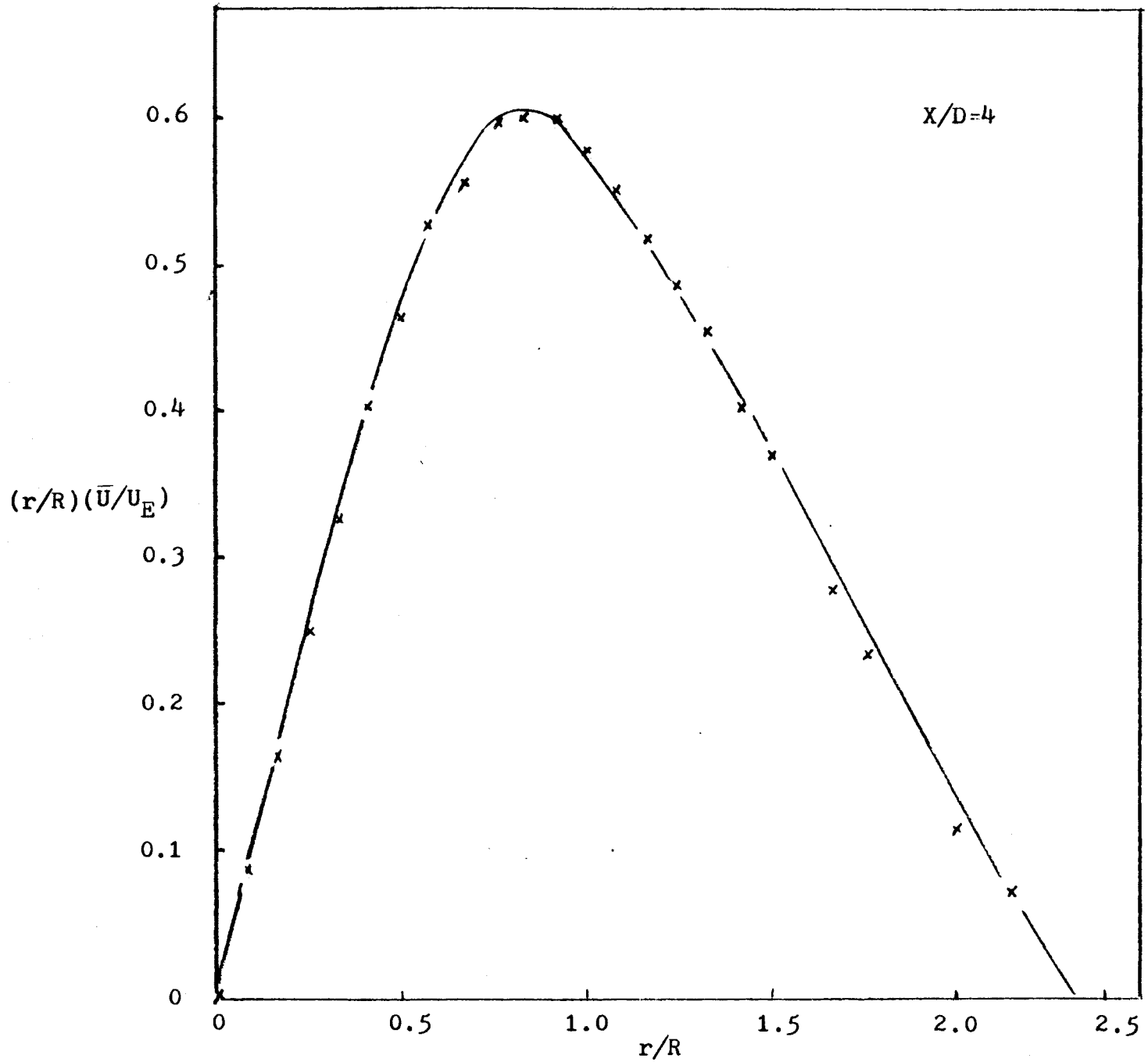
X/D=4
0.6
0.5
0.4
0.3
0.2
0.1
0
(r/R)(Ū/U_E)
0
0.5
1.0
1.5
2.0
2.5
r/R

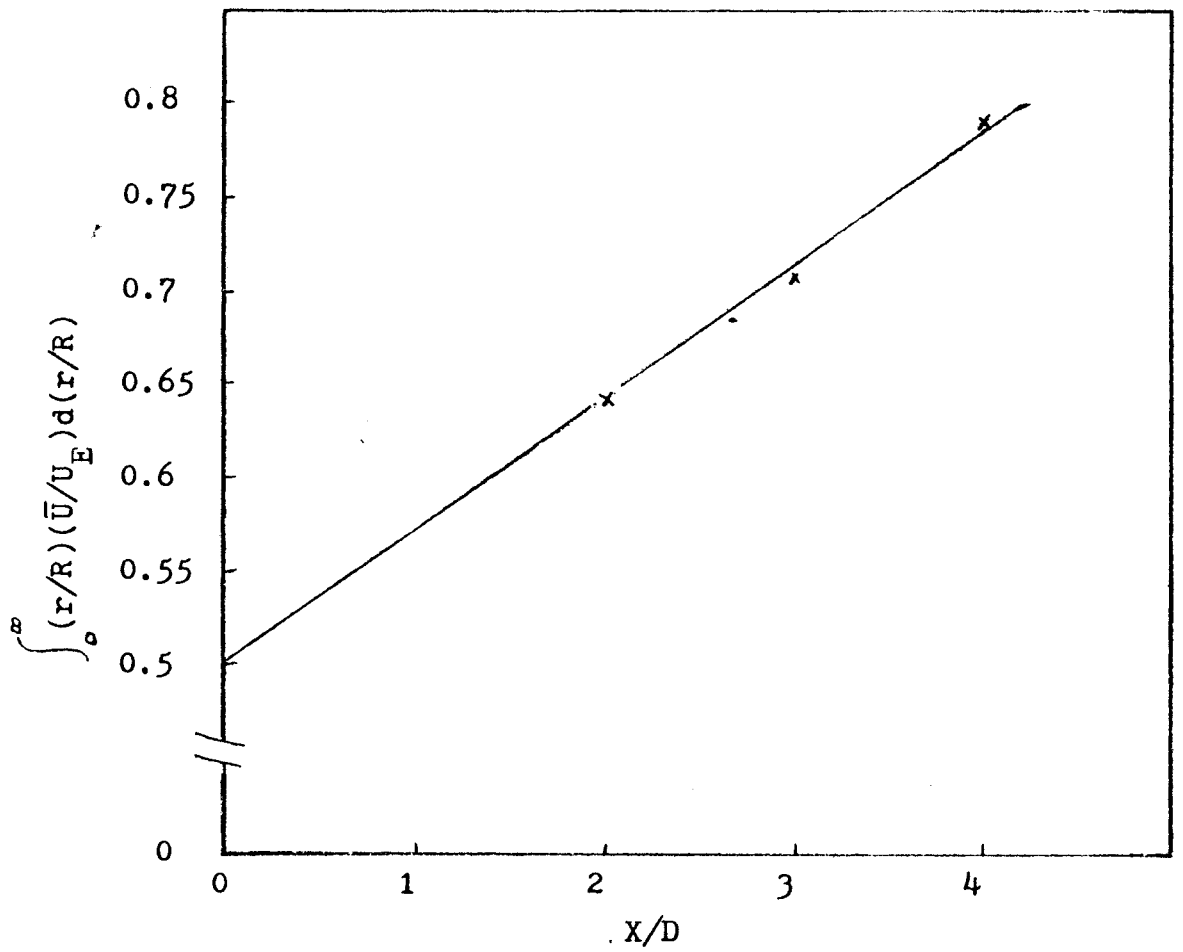

Fig. 6.9 Entrainment integral profile

thus

$$(rV)_\infty = -\frac{d}{dx}\int_0^\infty r'\,\bar{u}(r')\,dr' \qquad (6.10)$$

Thus we define the total entrainment rate, E, to represent the total volume of fluid added per unit length per unit time, and this given by

$$E = -2\pi\,(rV)_\infty \qquad (6.11)$$

Using Equ.(6.10), Equation (6.11) can be rewritten as

$$E = 2\pi\frac{d}{dx}\,\bar{u}_\ell R^2\int_0^\infty\left(\frac{r}{R}\right)\left(\frac{\bar{u}}{\bar{u}_\ell}\right)\frac{dr}{R}$$

$$= 2\pi\,\bar{u}_\ell R^2\frac{d}{dx}\int_0^\infty\left(\frac{r}{R}\right)\left(\frac{\bar{u}}{\bar{u}_\ell}\right)\frac{dr}{R} \qquad (6.12)$$

at the exit plane. The flow rate of the jet is

$$\dot{V}_0 = \pi\,\bar{u}_E R^2 \qquad (6.13)$$

in the first few diameters, therefore

$$\bar{u}_\ell \simeq \bar{u}_E$$

$$\therefore\ \frac{E}{\dot{V}_0} = 2\frac{d}{dx}\int_0^\infty\left(\frac{r}{R}\right)\left(\frac{\bar{u}}{\bar{u}_\ell}\right)\frac{dr}{R} \qquad (6.14)$$

multiplying by the jet diameter D on both sides yields the non-dimensionalized entrainment as

$$\frac{ED}{\dot{V}_0} = 2\frac{d}{d\left(\frac{x}{D}\right)}\int_0^\infty\left(\frac{r}{R}\right)\left(\frac{\bar{u}}{\bar{u}_\ell}\right)\frac{dr}{R} \qquad (6.15)$$

it follows from Equation(6.15) that

$$\frac{ED}{\dot{V}_0} = 0.138$$

thus for the axisymmetric jet mixing layer $\frac{ED}{\dot{V}_0} \simeq 0.14$, a result consistent with the approximate similarity of the flow in this region.

CHAPTER 7

SUMMARY AND CONCLUSION

The principal result of this investigation is that laser Doppler anemometer signal detection may be used for turbulent air flow measurements. However, a well-controlled seeding environment and an adjustable frequency shift are essential to obtain reasonable signal-to-noise ratio, especially when high turbulent intensity is encountered.

Doppler ambiguity arising from the random population ot scatterers has remained a primary source of data contamination in turbulent intensity and velocity spectra measurement. However, satisfactory results can be obtained from a single point LDA if care is taken to optimize the scattering parameters, the frequency shift and the signal processing.

Signal dropout is the major obstacle to using an analog tracking device in a highly turbulent flow. Care must be exercised in choosing a statistical averaging algorithm since the cause of the signal dropout has not yet been well developed. It is hoped that future research on this phenomenon will provide more insight about the problem.

The mixing layer measurements agreed well with the

established hot wire data, except at the outer edge where the hot wire data are suspect because of the high turbulence intensity. The data were shown to satisfy momentum conservation; however because of the flatness of the profile over most of the flow, this is not believed to be a very sensitive test of the accuracy of the velocity measurements, unlike in the fully developed jet. The entrainment rate was calculated for the first few diameter downstream of the axisymmetric jet and was found to be constant, as result consistent with the near-similarity of the velocity profiles.

REFERENCES

Arndt, R.E.A., Tran, N.C. and Barefoot, C.T. (1974) "Turbulence and Acoustic Characteristics of Screen Perturbed Jets" AIAA Journal, 12, 3, 261-262.

Baker, C.B. (1980) "Analysis of Turbulent Buoyant Jet" Ph.D. Dissertation, Pennsylvania State University, University Park, Pa.

Batchelor, G.K. (1953) "Theory of Homogeneous Turbulence", Cambridge Univ. Press, Cambridge,

Berman, N.S. and Dunning, J.W. (1973) "Pipe Flow Measurements of Turbulence and Ambiguity using Laser Doppler Velocimetry", J. Fluid Mech. V. 61, 2, 289-299.

Berman, N.W., "Fluid Particle Considerations in the Laser Doppler Velocimeter", Chap. 4. Short Course notes on the Laser Doppler Velocimeter. The Penn State University, University Park, Pa.

Beuther, P.D. (1980) "Experimental Investigation of Axisymmetric Turbulent Buoyant Plume" Ph.D. Dissertation, State University of New York at Buffalo, Buffalo, N. Y.

Bradshaw, P., Ferriss, D.H. and Johnson, R>F> (1964) "Turbulence in the Noise Producing Region of a Circular Jet", J. Fluid Mech., 19, 591-624.

Buchhave, P.,(1978) "Light Collecting System and Detector in a Laser Doppler Anemometry", Disa Information No. 15, 15-24.

Buchhave, P., (1978)"Errors and Correction Methods in Turbulence Measurement with an LDA", Ph.D Dissertation, State University of New York at Buffalo, Buffalo, N.Y.

Buchhave, P., (1978) "Bias Corrections in Turbulence Measurements by Laser Doppler Anemometer", Proc. 3rd Int. Workshop on Laser Velocimetry, July 11-13, Purdue Univ., W. Lafayette, Ind.

Buchhave, P., George, W.K., Jr. and Lumley, J.L., (1979) "The Measurement of Turbulence with the Laser Doppler Anemometer", Ann. Rev. Fluid Mech. 11, 443-503.

Caspersea, C.C. (1979) "Measuring the Flow-Field in Front of a Turbulent Nozzle Using Two-Color LDA." Disa Information No. 24, 5-8.

Durrante, T.S. and Greated, C.A. (1973) "Statistical Analysis and Computer Simulation of Laser Doppler Velocimeter Systems", Trans. IEEE, IM-22, 23-24.

Durst, F., Melling, A. and Whitelaw, J.H. (1976) "Principles and Practice of Laser Doppler Anemometry", New York Academic, 405 pp.

Edwards, R.V., Angus, T.C., French, M.J., Dunning, T.W., Jr. (1971) "Spectral Analysis of the Signal From Laser Doppler Flowmeter Time Independence System", J. Appl. Phys. 42, 837-850.

George, W.K., Jr. (1971) "An Analysis of theLaser-Doppler Anemometer and its Application to the Measurement of Turbulence", Ph.D. Dissertation, Johns Hopkins University, Laurel, Md.

George, W.K.,Jr., (1972) "Limitations on the Measurements of Unsteady Flow Velocities with a Laser Doppler Velocimeter", Fluid Dynamic Measurements in the Industrial and Medical Environment, Leicester Univ. Press.

George, W.K., Jr. and Berman, N.S. (1973)"Doppler Ambiguity in Laser Doppler Velocimeters", Appl. Phys. Lett., V.23, No.5.

George, W.K., Jr. and Lumley, J.L. (1973) "The Laser Doppler Velocimeter and its Application to the Measurement of Turbulence." J. Fluid Mech. 60, 321-362.

George, W.K., Jr. (1974) "The Measurement of Turbulence Intensities Using Real-Time Laser Doppler Velocimetry", J. Fluid Mech. 66, 11-16.

George, W.K., Jr. (1976) "Limitations to Measuring Accuracy Inherent in the Laser-Doppler Signal". See Asalor _Whitelaw (1976) pp. 20-63.

George, W.K., Jr. (1979) "Processing of Random Signals", Proc. of the Dynamic Flow Conf. 1978. PO Box 121, DK-274, Skovlunde, Denmark, 757-800.

George, W.K., Jr. (1980) Presentation at Meeting of Principals of the Cooperative Investigation of Jet Noise, IIT, Chicago, Ill.

George, W.K., Jr., Beuther, P.D. and Arndt, R.E.A. "Pressure Spectra in Turbulent Free Shear Flows". To be published in J. Fluid Mech.

Greated, C. and Durranti, T.S. (1971) "Signal Analysis for Laser Velocimeter Measurements", J. Phys. E. V.4, 24-26.

Hinze, J.O. (1975) "Turbulence", McGraw-Hill Publ.

Hussain, A.K.M.F. and Zedan, M.F. (1978) "Effect of the Initial Condition on the Axisymmetric Free Shear Layer", Phys.of Fluids, V.21, Nos. 7 and 9.

Khwaja, M.S.S. (1981) "Investigation of the Turbulent Axisymmetric Jet Mixing Layer", M.S. Thesis, Department of Mech. _Aero. Engr., State University of New York at Buffalo, Buffalo, N.Y.

Lading, L. (1973) "Analysis of Signal-to-Noise Ratio of the Laser Doppler Velocimeter", Opto Electronics, V.5, 175-187.

Lading, L. and Edwards, R.V. (1976) "The Effect of Measurement Volume on Laser-Doppler Anemometer Measurements as Measured on Simulated Signals". See Asalor and Whitelaw, pp. 64-80.

Lumley, J.L.,(1957) "Some Problems Connected With the Motion of Small Particles in Turbulent Fluid", Ph.D. Dissertation, Department of Mech. Engr., The Johns Hopkins University, Laurel, Md.

Lumley, J.L., George, W.K., Jr. and Buchhave, P. (1978) "Influence of Refractive Index Fluctuation on Velocity Measurements with an LDA". To be submitted for publication in Physics of Fluids.

Lumley, J.L., Buchhave, P. and George, W.K. (1978) "Influence of Drop-out on Velocity Measurements with Continuous LDA". To be submitted for publication in Physics of Fluids.

Melling, A and Whitelaw, J.H.,(1973) "Seeding of Gas Flows for Laser Anemometry", Disa Information No. 15, 5-14.

Monin, A.S. and Yaglom, A.M. (1965) "Statistical Fluid Mechanics, Mechanics of Turbulence", V1, MIT Press.

Nagib, H.M. (1980) Presentation at the meeting of principals of the Cooperative Investigation of Jet Noise , Illinois Institute of Technology, Chicago, Ill.

Siegman, A.E., Appl. Optics 5, 10, pp. 1588-1594, 1966.

Tchen, C.M., (1947) "Mean Value and Correlation Problems Connected with the Motion of Small Particles in a Turbulent Fluid". (Dissertation, 1947 - Delft) The Hague, Martinus Nijhoff.

Tennekes, H. and Lumley, J.L. (1972) "A First Course in Turbulence", M.I.T. Press, Cambridge.

Tran, N.C.,(1973) "Turbulence and Acoustic Characteristics of a Screen Perturbed Jet", M.S. Thesis, The Pennsylvania State Univ.

Wygnanski, I., Fiedler, H. (1969) "Some Measurements in the Self-Preserving Jet", J. Fluid Mech. 38, 3, 577-612.

APPENDIX: TRACKER PROGRAM LISTING

```
==========TRACK.FOR==========

=========13-DEC-80==========

      PROGRAM TRACK
      COMMON /PARAMW/IBW,IRANGE
      DIMENSION RANGE(7)
      REAL MVEL(100),LOCK(100),MSQVEL(100),LCOEFF(100),MSQL(100)
     *,MV1(100),MSQV1(100)
C
      CALL PARAM
      TYPE 75, IBW,IRANGE
75    FORMAT(1H1,5X,'IBW=',I1,5X,'IRANGE=',I1,//)
76    TYPE *, 'ENTER NUMBER OF SAMPLES PER BLOCK.'
      ACCEPT *,NUM
      IF(NUM .LE. 5000) GO TO 77
      TYPE *, 'NUMBER TOO LARGE. TRY AGAIN.'
      GO TO 76
77    CONTINUE
78    TYPE *, 'ENTER NUMBER OF BLOCKS (100 MAX.).'
      ACCEPT *, NBLOCK
      IF (NBLOCK .LE. 100) GO TO 79
      TYPE *, 'NUMBER OF BLOCKS TOO BIG, TRY AGAIN.'
      GO TO 78
79    CONTINUE
C
      TYPE *, 'DO YOU WANT DATALIST FOR EACH SAMPLE? YES=1,NO=0'
      ACCEPT *, K0
      TYPE *, 'DO YOU WANT DATA LIST FOR EACH BLOCK? YES=1,NO=0'
      ACCEPT *, K2
C
      PAUSE 'TO START SAMPLING, HIT RETURN !'
C
C     NBLOCK OF SAMPLING BEGINS AND AVERAGES FOR EACH BLOCK FORMS
C
      DO 1000 J=1,NBLOCK
```

```
      CALL COLLEC(NUM,0,0,1,2)
      TYPE *, 'DATA COLLECTION FOR BLOCK NO. ',J,' IS FINISHED.'
      TYPE *, ' '

      RANGE(1) = 1.E4
      RANGE(2) = 3.3333E4
      RANGE(3) = 1.E5
      RANGE(4) = 3.3333E5
      RANGE(5) = 1.E6
      RANGE(6) = 3.3333E6
      RANGE(7) = 1.E7

      XMV1=0.
      XMSV1=0.
      NUM1=0
      XMVEL=0.0
      XMSVEL=0.0
      MLOCK=0
      CORR=0.0

      INTERNAL DATA FORMAT CONVERSION BEGINS AND
      FREQ. AND CORRELATION CALCULATION FOLLOWS FOR EACH SAMPLE

      DO 100 I=1,NUM
      KOUNT=I
      CALL TRANST(1,KOUNT,IVEL,LOK)
      U = (FLOAT(IVEL)/256.) * RANGE(IRANGE)
      L = LOK
      K1=K0
      IF(K1 .EQ. 0) GO TO 91
      TYPE 85
      TYPE 80, KOUNT,IVEL,LOK,U,L
      FORMAT(1H ,5X,'COUNT',4X,'IVEL',4X,'LOCK',4X
     *,'TRACKER FREQ',4X,'L')
      FORMAT(1H ,6X,I4,4X,I4,5X,I1,6X,E12.3,4X,I1,//)
      CONTINUE

      Compute moments from data

      IF(L .EQ. 0)GO TO 92
      XMV1=XMV1+U
      XMSV1=XMSV1+U**2.
      NUM1=NUM1+1
      GO TO 93
      XMV1=XMV1+0.
      XMSV1=XMSV1+0.
      NUM1=NUM1+0
      MLOCK=MLOCK+L
      XMVEL=XMVEL+U
      XMSVEL=XMSVEL+U**2
      CORR=L * U + CORR
```

```
0     CONTINUE

      COMPUTE MEAN QUANTITIES

      MV1(J)=XMV1/FLOAT(NUM1)
      XMSV1=XMSV1/FLOAT(NUM1)
      LOCK(J)=FLOAT(MLOCK)/FLOAT(NUM)
      MVEL(J)=XMVEL/FLOAT(NUM)
      XMSVEL=XMSVEL/FLOAT(NUM)
      CORR = CORR/FLOAT(NUM)

      COMPUTE CORRELATION COEFFICIENT

      XSMV1 = MV1(J)**2
      MSQV1(J) = XMSV1-XSMV1
      XSMVEL = MVEL(J)**2
      MSQVEL(J) = (XMSVEL - XSMVEL)
      MSQL(J)= LOCK(J)*(1.-LOCK(J))
      LCOEFF(J)= CORR- LOCK(J)*MVEL(J)
      IF(MSQV1(J) .LT. 0.)GO TO 108
      XVRMS1 = SQRT(MSQV1(J))
      GO TO 109
8     XVRMS1 = -(SQRT(ABS(MSQV1(J))))
9     IF(MSQVEL(J) .LT. 0.)GO TO 110
      XVRMS = SQRT(MSQVEL(J))
0     IF(MSQL(J) .LT. 0.)GO TO 130
      XLRMS = SQRT(MSQL(J))
      GO TO 131
0     XVRMS= -(SQRT(ABS(MSQVEL(J))))
      GO TO 120
0     XLRMS= -(SQRT(ABS(MSQL(J))))
1     CONTINUE
      DIV = XLRMS * XVRMS
      IF(DIV .EQ. 0.) GO TO 899
      COEFF = LCOEFF(J) / DIV

      Output data

      K3=K2
      IF(K3 .EQ. 0) GO TO 1000
      IJ=J
      TYPE *, 'DATA FOR BLOCK:', IJ
      TYPE 700, MVEL(J),MV1(J)
0     FORMAT(1H1,10X,'MEAN FREQ=',E12.3,2X,',',2X,
     *'ABS MEAN FREQ=',E12.3)
      TYPE 750, XVRMS,XVRMS1
0     FORMAT(1H ,10X,'RMS  FREQ=',E12.3,2X,',',2X,
     *'ABS. RMS FREQ=',E12.3)
      TYPE 800, COEFF
0     FORMAT(1H ,10X,'CORRELATION COEFFICIENT=',E12.3)
```

```
      TYPE 850, LOCK(J)
0     FORMAT(1H ,10X,'MEAN LOCK=',E12.3)
      TYPE *, ' '
00    CONTINUE


      XMEAN=0.
      XLOCK=0.
      XRMS=0.
      XCOEFF=0.
      XMSQL=0.
      XMEAN1=0.
      XRMS1=0.

      COMPUTE SUM OF EACH QUANTITY FOR ALL BLOCKS

      DO 1001 K=1,NBLOCK
      XMEAN1=XMEAN1+MV1(K)
      XRMS1=XRMS1+MSQV1(K)
      XMEAN= XMEAN+MVEL(K)
      XLOCK= XLOCK+LOCK(K)
      XRMS= XRMS+MSQVEL(K)
      XCOEFF= XCOEFF+LCOEFF(K)
      XMSQL= XMSQL+MSQL(K)
01    CONTINUE

      COMPUTE MEAN FOR EACH QUANTITY AND FORM
      CORRELATION COEFFICIENT FOR ALL BLOCKS

      XMEAN1= XMEAN1/FLOAT(NBLOCK)
      XMEAN= XMEAN/FLOAT(NBLOCK)
      XLOCK= XLOCK/FLOAT(NBLOCK)
      IF(XRMS1 .LT. 0.) GO TO 401
      XRMS1= SQRT(XRMS1/FLOAT(NBLOCK))
      GO TO 402
1     XRMS1= -(SQRT(ABS(XRMS1/FLOAT(NBLOCK))))
2     IF(XRMS .LT. 0.) GO TO 410
      XRMS= SQRT(XRMS/FLOAT(NBLOCK))
0     IF(XMSQL .LT. 0.) GO TO 430
      XMSQL= SQRT(XMSQL/FLOAT(NBLOCK))
      GO TO 431
0     XRMS= -(SQRT(ABS(XRMS/FLOAT(NBLOCK))))
      GO TO 420
0     XMSQL= -(SQRT(ABS(XMSQL/FLOAT(NBLOCK))))
1     CONTINUE
      XCOEFF= XCOEFF/FLOAT(NBLOCK)/(XRMS*XMSQL)

      TYPE 10
      FORMAT(1H1,///)
      TYPE *, 'AVERAGES FOR ALL BLOCKS.'
      TYPE *, 'MEAN          FREQENCY  :',XMEAN
```

```
TYPE *, 'ABSOLUTE MEAN FREQENCY  :',XMEAN1
TYPE *, 'R.M.S.          FREQENCY :',XRMS
TYPE *, 'ABSOLUTE R.M.S. FREQENCY:',XRMS1
TYPE *, 'MEAN                LOCK  :',XLOCK
TYPE *, 'CORRELATION COEFFICIENT :',XCOEFF

TYPE *, '( DIV IS TOO SMALL, FLOATING ZERO DIVIDE WOULD INCUR )'

TYPE 900
FORMAT(1H2,5X,'RERUN THE PROGRAM?  YES=1,NO=0')
ACCEPT *, K
IF(K.EQ.1)GO TO1
TYPE *, 'PROGRAM TRACK COMES TO AN END!'
END
```

Note: Subroutine COLLEC and TRANST are data acquisition programs supplied by Disa Electronics.

```
================SUBROUTINE PARAMETER (FOR TRACKER)==================

================DEC-6-1980==========================================
    SUBROUTINE PARAM
    COMMON /PARAMW/IBW,IRANGE
    TYPE *, 'PROGRAM PARAM SETS THE BANDWIDTH AND RANGE'
    TYPE *, 'SELECT BANDWIDTH(0-3) AND RANGE(1-7) AS FOLLOW:'
    TYPE *, 'BW1=1,BW2=2,BW3=3,BW(INFINITY)=0'
    TYPE *, 'RANGE : 1-10KHZ = 1,----,RANGE : 1-10MHZ =7'
    TYPE *, 'SET BANDWIDTH AND RANGE [I1,I1]'
    ACCEPT *, IBW,IRANGE

    TRANSFER THE PARAMETERS TO SET THF TRACKER BANDWIDTH & RANGE

    CALL PARA(IBW,IRANGE)
    RETURN
    END
```

```
============SUBPROGRAM PARAMETER (FOR TRACKER)==================

HIS SUBPROGRAM IS CALLED BY PARAM.FOR WHICH WILL TRANSFER THE
ANDWIDTH AND RANGE SETTINGS ACCORDING TO USER'S SELECTION

=============DEC-6-1980=========================================

        .TITLE  PARA
        .GLOBL  PARA
        OUTBUF=167772
        CHAN=60000

RA:     ADD     #2,R5           ;CORRECT POINTER
        MOV     @(R5)+,R1       ;TRANSFER BANDWIDTH
        SUB     #1,R1           ;NORMALIZE
        BIC     #177774,R1      ;CLEAR NONRELAVENT BIT
        ASL     R1              ;SHIFT LEFT 3 TIMES
        ASL     R1
        ASL     R1
        MOV     @(R5)+,R2       ;TRANSFER RANGE
        BIC     #177770,R2      ;CLEAR NONRELAVENT BIT
        BIS     R2,R1           ;PUT INFORMATION TOGETHER
        SWAB    R1              ;CORRECT POSITION
        ASR     R1              ;MOVE 7 BITS TO THE RIGHT
        BIS     #CHAN,R1        ;SET OUTPUT ADDRESS
        MOV     R1,@#OUTBUF     ;SET THE TRACKER'S SWITCH
        RTS     PC              ;END OF SUBPROGRAM
        .END    PARA
```